AFFDL-TR-71-4
PART II

AIR-CUSHION PRESSURE DURING STIFF-OPERATION FOR AIR-CUSHION LANDING SYSTEMS

PART II. EXPERIMENTS

LIT S. HAN

THE OHIO STATE UNIVERSITY RESEARCH FOUNDATION
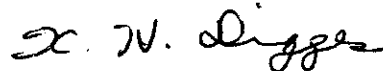
FOREWORD

This is Part II of the investigation on the air-cushion pressure during stiff-operation of ACLS Systems and details the experimental verification of the theory developed in Part I (Theory). In addition a parallel experimental program was conducted to calibrate the discharge coefficients for a matrix of orifices in triangular and square patterns at various pitch ratios. The work reported herein was sponsored by the Air Force Flight Dynamics Laboratory, USAF under contracts AF 33(615)-69-C-1001 and F 33(615)-70-C-1019 with The Ohio State University Research Foundation.

Acknowledgement is hereby made to the contributions by Mr. Albert Dickerson who took care in the design and construction of the cushion chamber and analyzed much of the experimental data. Mr. Gregory Bozin undertook the work of orifice calibration. The reported experimental work was completed July 1971 and analysis and compilation were concluded January 1972. Manuscript of the report was released March, 1972.

This report has been reviewed and approved.

KENNERLY H. DIGGES
Chief, Mechanical Branch
Vehicle Equipment Division
AF Flight Dynamics Laboratory

ABSTRACT

This Part II of the report describes the experimental verification of the theory developed in Part I for ACLS in its stiff-mode operation. It also reports the discharge coefficient data required for computing air flow requirements.

At low ground clearances, the theory was verified to be in excellent agreement with the experimental data obtained. At higher values of the ground clearance where the viscous flow theory is not expected to hold, appreciable difference between the experimental data and theoretical computation was observed. A multi-jet theory yet to be developed is expected to bridge the gap.

CONTENTS

LIST OF FIGURES AND TABLES

LIST OF FIGURES AND TABLES (CONT'D)

LIST OF FIGURES AND TABLES (CONT'D)

I.   INTRODUCTION

This is Part II of a two-part report which is concerned with the air cushion pressure of an ACLS (Air-Cushion Landing System) during a stiff-mode operation. In Part I, an analysis was completed to study the flow velocity distribution of the injected air in the clearance space between the ground and supply chamber. The particular physical configuration used to simulate such a stiff-mode operation is depicted in Figure 1 which also appeared in Part I. It is essentially a two-dimensional flow model in which the cushion air is forced through a series of orifice holes located at the bottom of a pneumatic bag. The supply bag is off the ground with a clearance H and is in almost parallel configuration with the ground surface over a length of L.

Because of the fact that in the cushion air space the air motion is secondary, i.e. it is induced by the air injection near the ground plane, a simplified mathematical model was adopted in which the two sides of the injection lengths (total 2L) were brought together and formed a continuous path through which air was assumed to be injected in a continuous manner. Such a mathematical model is shown in Figure 2 which also appeared in Part I of this report. The computed pressure at $x = 0$ is then taken as the pressure in the stagnant cushion space in Figure 1 .

1

The first phase of study completed in Part I was concerned with the case of uniform injection rate over the top plate (bottom of supply chamber in Figure 1) of the flow channel shown in Figure 2. The distribution of the velocity parallel to the ground was calculated over a large range of the injection Reynolds number. The pressure gradient along the main flow direction was also determined as a function of the Reynolds number. In the second phase of the theoretical study, the rate of air flow from the supply chamber to the ground clearance space was considered variable in such a fashion that the air flow rate was dependent upon the difference between the supply (trunk) pressure and the local air pressure in the flow channel. In addition, an orifice coefficient was introduced to denote the contraction effects which would normally exist under this kind of flow restrictions. A method of calculation was developed which was simple in concept but repetitious in execution. In order to simplify its operation, a computer program was developed which will execute all the necessary operations. In short, the computer program requires the following inputs:

(i)   "Footprint" length L (feet)

(ii)   Ground clearance H (feet)

(iii)   Bleed hole density A_r (ratio)

(iv)   Orifice coefficient C_d (discharge coefficient)

(v)   Supply and ambient pressures (psia)
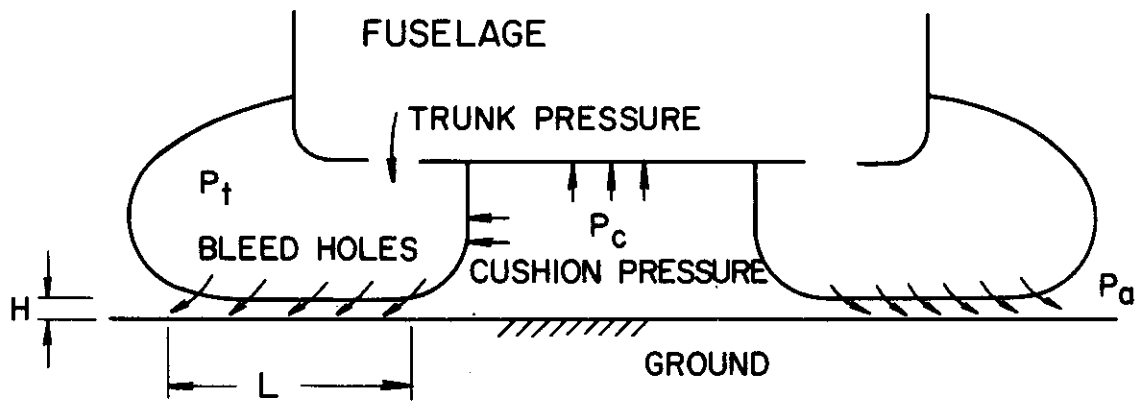
FIGURE I. SCHEMATICS OF AIR-CUSHIONED
LANDING SYSTEM
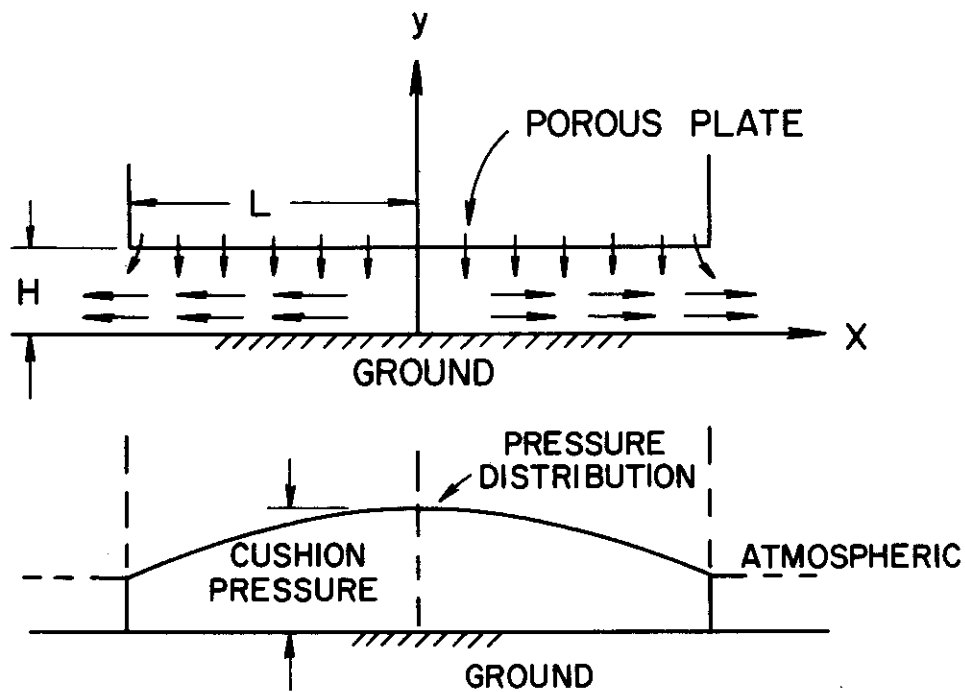
FIGURE 2. SIMPLIFIED FLUID DYNAMIC MODEL
FOR STIFF OPERATION

The outputs of the computer program consist of the following
items:

(a) Pressure in the air cushion space.

(at x = 0, Figure 2)

(b) Pressure variation along the ground clearance
path.

(c) The total air flow per foot of depth.

II. EXPERIMENTAL OBJECTIVES

In the theoretical part, a major assumption was
that the cushion air forced through the orifices from the
supply chamber can be simulated by a continuous flow pattern
along the top of the flow channel shown in Figure 2. The
ratio A_r of the orifice or hole area to the total gross area
is therefore the pro-rata ratio in order to have the same
total flow quantity. Additionally, the assumption of incom-
pressible, viscous, laminar flow was also adopted. As in
all theories, experimental check is necessary in order to
have confidence in its application to design. Consequently
the main purpose of this work was to verify the theory
developed in Part I.

A second objective was to determine the orifice
discharge coefficient C_d necessary in calculating flow
through the orifice assembly. This is particularly important
for the theory developed in Part I, since an accurate

evaluation of C_d is necessary for a reliable prediction of the cushion pressure ratio. It is significant to observe that in previous research concerning hovercraft a commonly used configuration is the periphery jet as illustrated in Figure 3a in which an air stream was formed along an upstream guiding channel. The air jet emerging from the flow channel would maintain the same jet width. In this event the discharge coefficient would be equal to one. However, in ACLS work such a physical configuration is not practical and instead a series of orifice holes is usually provided on the supply chamber. The flow just outside the orifice would assume the pattern in Figure 3b in which there is a necking-down of the air stream. The discharge coefficient would then be less than one.
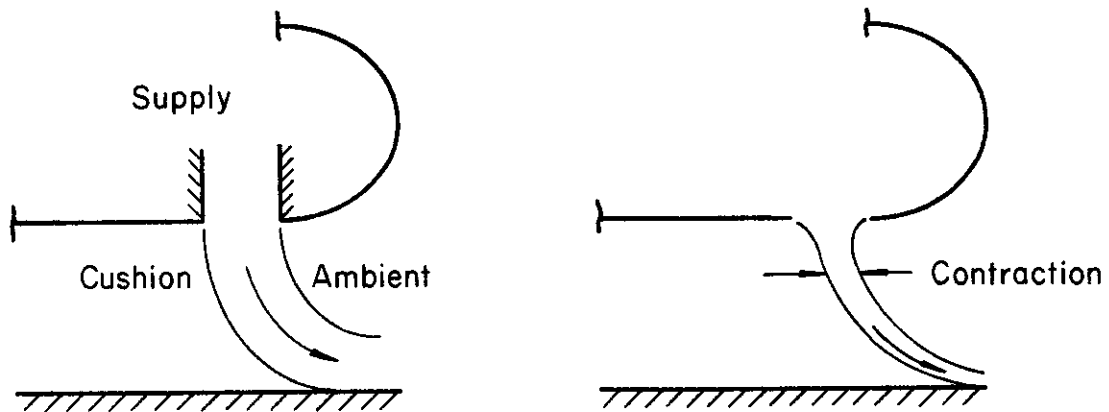
(a) Hovercraft Periphery Jet   (b) ACLS Orifice Jets

Figure 3. Jet Contractions for Hovercraft and ACLS Applications

It is commonly known that in the case of a single orifice the discharge coefficient C_d is in the vicinity of of 0.6. The values of C_d have been experimentally investigated in the past in connection with flow metering work. The numerical values were well documented in ASME Fluid Meters Publications (Fluid Meters - Their Theory and Application, Am. Soc. of Mech. Engrs., New York, 1959). However, in ACLS work the orifices are grouped in close proximity with one another. It is therefore expected that there will be a modification of the single orifice data to ACLS application where the orifices may be arranged in square, or triangular pitch patterns. For this reason, a series of experimental runs were made to determine the discharge coefficients C_d for various orifice arrangements. This part of the work is detailed in Appendix I of this report.

III. CUSHION PRESSURE EXPERIMENTATION

a. Apparatus

In order to simulate the stiff-mode operation of ACLS as depicted in Figure 1, the major components of test apparatus consist of a flat-bottomed air supply chamber adjacent to an enclosed cushion space. The supply chamber was equipped with a removable bottom panel which was in reality an orifice plate with holes at a chosen pitch.

All of these bottom panels had dimensions of 12.75 inches
and 18.75 inches. The smaller dimension (12.75 inches)
was oriented in the direction of main air flow. The larger
dimension (18.75 inches) was along the direction of no-flow.
In principle this latter dimension should be as large as
possible to approximate the two-dimensional character of
flow field. However, experimental results, to be mentioned
later, confirmed that this dimension was adequate. The
general layout of these two major components is shown in
Figure 4.

The cushion and supply chambers were both made
of plywood (1/2 inch thick) and on the side walls of the
cushion chamber plexi-glass windows were provided to observe
the air recirculation patterns as indicated by thread tufts
attached to the interior walls. The walls were sand-papered
to have a smooth surface free from burrs and high spots.
Altogether 63 static pressure openings of 3/16-inch diameter
were located along the bottom, back and top of the cushion
space. These tap openings were located on three different
rows shown in Figure 5. At the ground board directly below
the supply chamber orifice plate, static pressure openings
numbered one through seven were located about two inches
apart and on the remaining periphery they were six inches
apart.

Pressure Taps,Three Rows

Air Supply From Compressor
And Metering Section

Cushion Chamber

Supply Chamber
(internal baffle
not shown)

Orifice Plate

18.75"

24"

12.75"

54"

24"

Observation
Windows
(plexiglass)

Ground Board
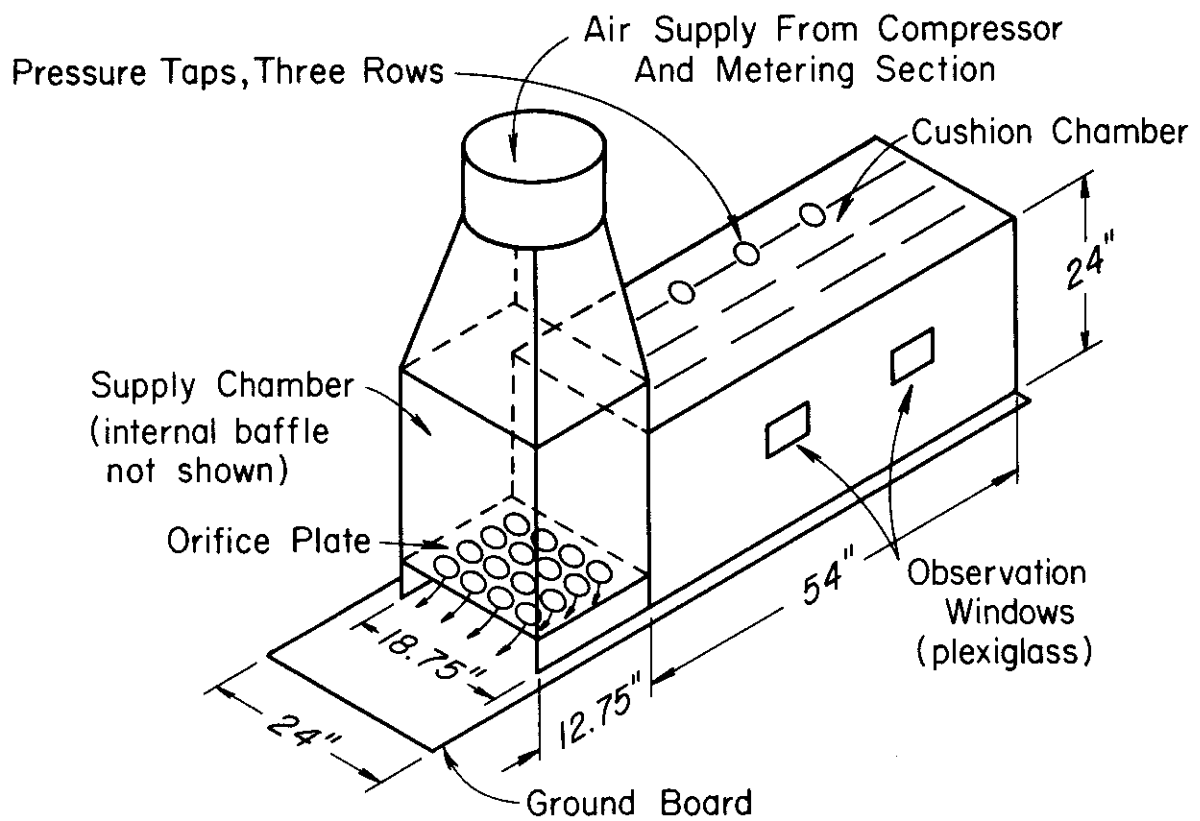
FIGURE 4. Schematics of Test Assembly
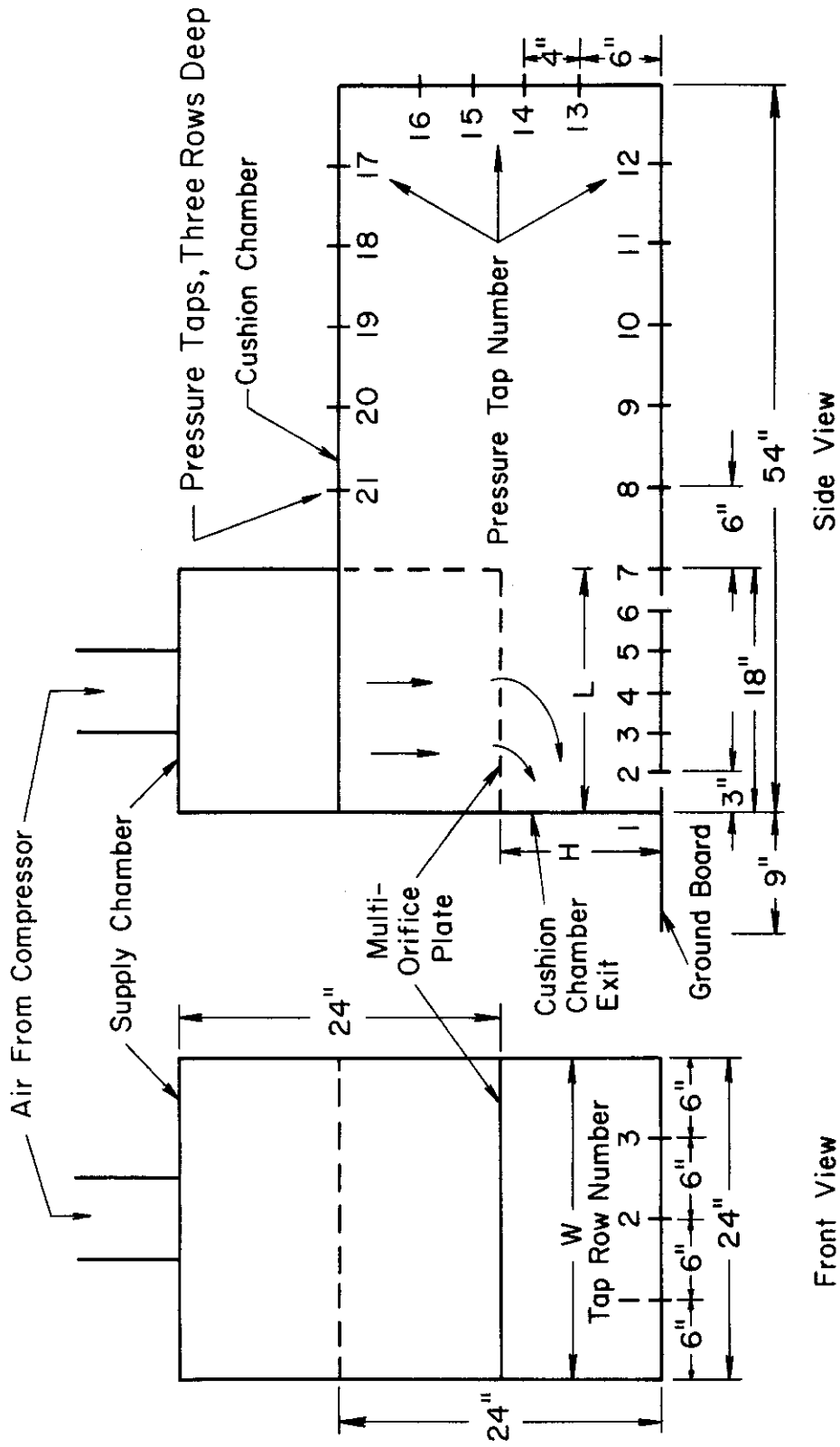
FIGURE 5. Front and Side View of Test Apparatus

The supply chamber had a four-inch diameter inlet through which air was supplied from the compressor. Underneath the inlet and inside the chamber was a baffle plate and two screens, located five and ten inches below the top of the supply chamber. The baffle plate and screens were used to provide a uniform flow toward the bottom of the chamber. At the bottom of the supply chamber a multi-orifice plate was attached by screws. The inside dimensions of the supply chamber were 18.75 inches wide (no-flow direction) and 12.75 inches deep (main-flow direction) as compared with the outside dimensions of 24 inches wide and 18 inches deep. This area reduction was due to internal braces to which the orifice plate was attached. A Pitot tube (one-eighth inch outer diameter) was inserted in the front side of the supply chamber five inches above the bottom of the chamber and ten inches from the left side of the chamber. This location was chosen so that the Pitot tube readings would not be affected by any flow irregularities caused by the screens inside the chamber, the orifice plate, or the side walls. The supply chamber had two angle iron braces bolted horizontally across the front of the chamber and two flat iron braces bolted vertically to the back of the chamber. These braces were either bolted or clamped to the cushion chamber so that the supply chamber could be moved vertically up or down relative to the ground board

of the cushion chamber. The supply chamber was raised and lowered by means of a mechanical lift. By bolting or clamping the chambers together at four points, it was always possible to keep the orifice plate of the supply chamber parallel to the ground board of the cushion chamber.

b. Multi-Orifice Plates

A picture of the three multi-orifice plates used in this experiment is shown in Figure 6. All three plates were 24 inches wide and 18 inches in depth. They were made of either aluminum plate or steel sheet metal. The plates are classified according to their area ratio, the orifice area to the total plate area. The first plate had seventy holes of 1.1875-inch diameter, arranged in seven rows of ten holes each. The holes were arranged in a square pattern such that the centerline of the holes were spaced two inches apart. This plate had an area ratio of 0.180. The second plate had the same hole arrangement as the first but the holes were only 0.9375 inches in diameter. The area ratio of this plate was 0.112. The third plate had 228 holes of 0.3800-inch diameter arranged in twelve rows of nineteen holes each. The holes were again arranged in a square pattern but the centerline of the holes were spaced one inch apart. This plate had an area ratio of 0.060. The first two plates were used to ascertain the effect of different area

11
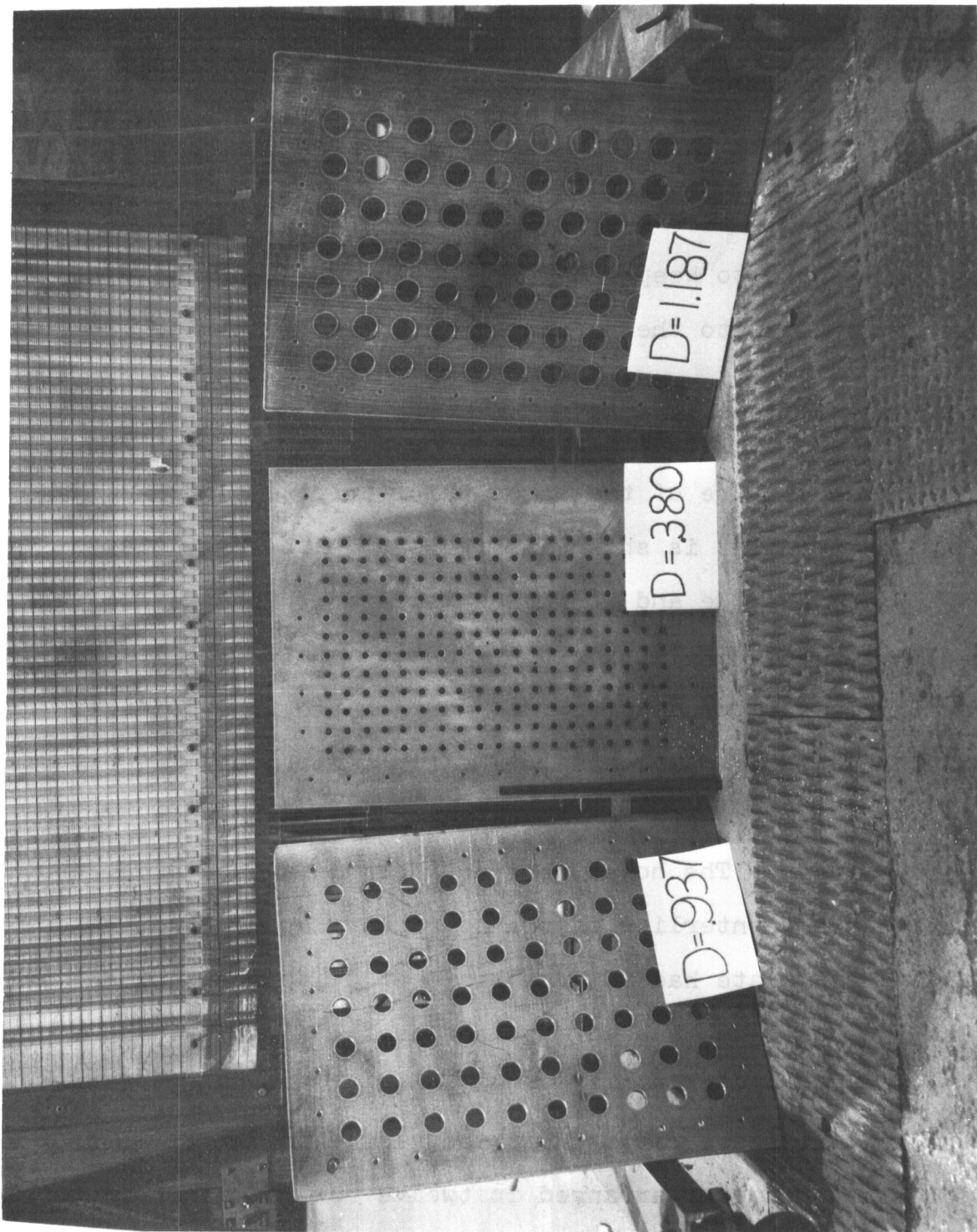
Figure 6   Multi-Orifice Plates

ratio with the same hole arrangement. The third plate
was used to ascertain the effect of a different area ratio
as well as a different hole arrangement. The geometrical
characteristics of the multi-orifice plates were listed
in Table 1.

Table 1

Geometrical Characteristics of the Multi-Orifice Plates

Plate Number	Hole Diameter (inches)	Center-Center Distance (inches)	Area Ratio* A_r
1	1.1875	2.0	0.180
2	0.9375	2.0	0.112
3	0.3800	1.0	0.060

* A_r = area of orifice holes/plate-area.

c. Air Supply

The air was supplied to the test apparatus by a
Fuller vane air compressor capable of delivering 1800 cfm
of standard air. The air from the compressor was fed into
a reservoir where the pressure was maintained at a maximum
of 40 psig. The air flowed out of the storage tank through
an eight-inch diameter pipe. The piping was then reduced to
a six-inch and then a four-inch diameter pipe. The flow
rate of the air was controlled by three valves, one of which
was a bypass valve on the storage tank and the other two

were a gate value and globe valve located at two points along
the four-inch section of the pipe. The flow rate was
measured by means of a standard orifice plate (diameter
ratio of 0.5275) located in the four-inch section. A three-
foot piece of flexible hose connected the four-inch pipe to
the top of the supply chamber. The flexible hose was
adjusted whenever it was necessary to raise or lower the
supply chamber.

d.   Instrumentation

The mass flow rate of the supply air was measured
in the four-inch section of the pipe by means of a square-
edged orifice plate with flanged taps. The diameter ratio
of the orifice plate was 0.5275. It was chosen so that the
range over which the flow rate was varied throughout the test
could be measured by the use of either a twelve-inch U-tube
mercury manometer or a sixty-inch well-type water manometer.
Both manometer scales were divided into tenth-of-an-inch
intervals. The air temperature in the pipe was measured by
a 120°F liquid-in-glass thermometer. This thermometer was
similar to the thermometers used to measure the ambient
temperature as well as the temperature in the cushion chamber.
The scale of the thermometer was divided into one-degree
intervals. The static pressure of the air in the pipe was
measured by a 60-psi Bourdon pressure gage which was divided

into one-psi intervals. A dead-weight-gage calibration was used to calibrate the Bourdon gage. The atmospheric pressure was measured by a single-leg mercury barometer divided into tenth-of-an-inch intervals.

The pressure distribution on the cushion chamber surface was measured by fifty water manometers connected to a common well and can be seen in Figures 7 and 8. The scale of the water manometers was divided into tenth-of-an-inch intervals. A one-inch and a three-inch Ellison draft gages were also used to measure the cushion pressure to obtain a more accurate reading at low pressures. The scales on both draft gages were divided into hundredth-of-an-inch intervals. A Pitot-static tube, twelve inches in length, one-eighth of an inch in diameter and two inches long at the stem, was used to measure the total pressure in the supply chamber and to measure the exit velocity profile out of the cushion chamber. The pressure readings from the Pitot tube were either measured by the three-inch draft gage, or when it went off scale, by a water manometer. The height of the plenum chamber above the ground board was measured by a twelve-inch scale which was divided into hundredth-of-an-inch intervals. The general standard established by the American Society of Mechanical Engineers was used to determine the characteristics of a Pitot-static tube.
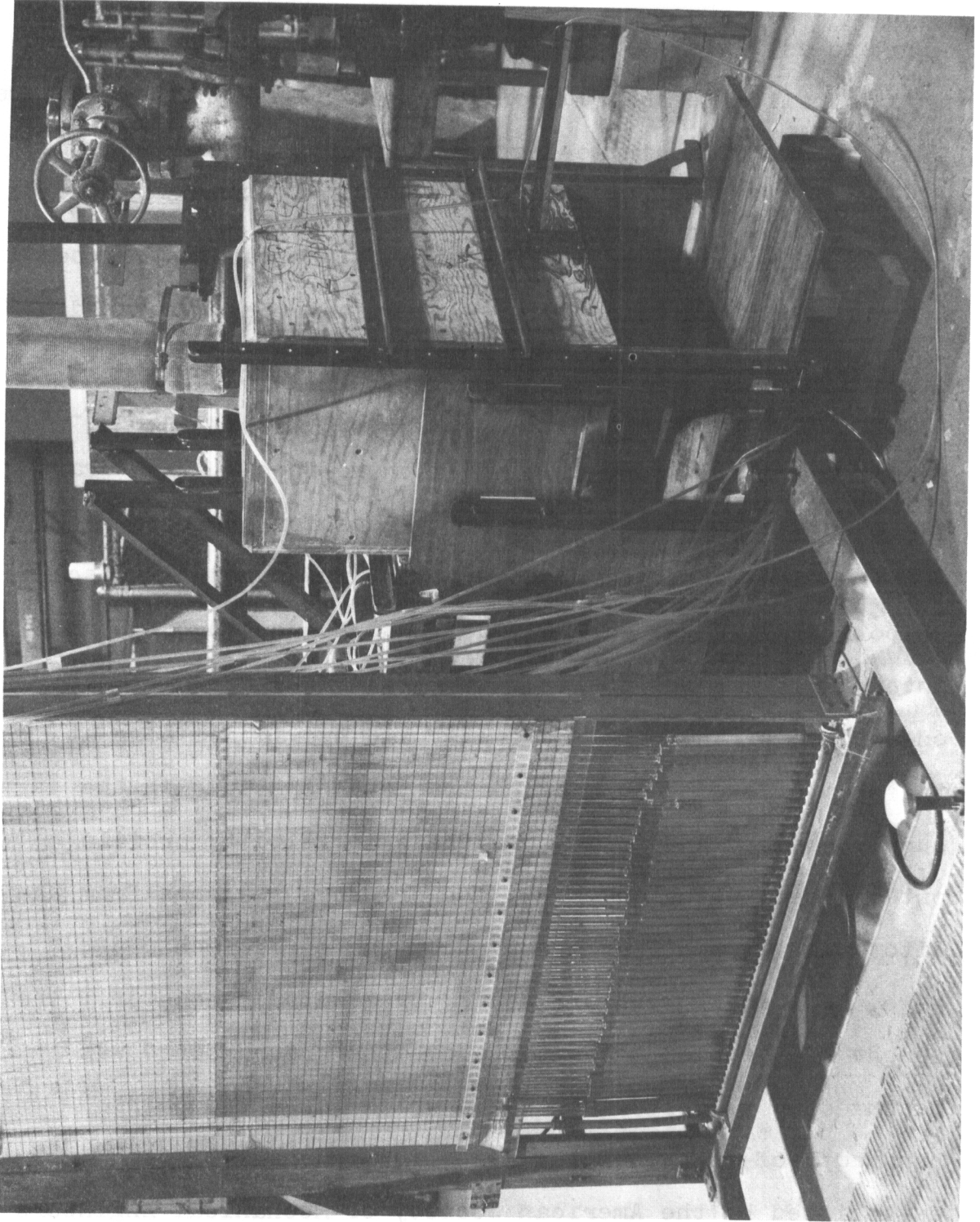
Figure 7   Side View of Test Assembly
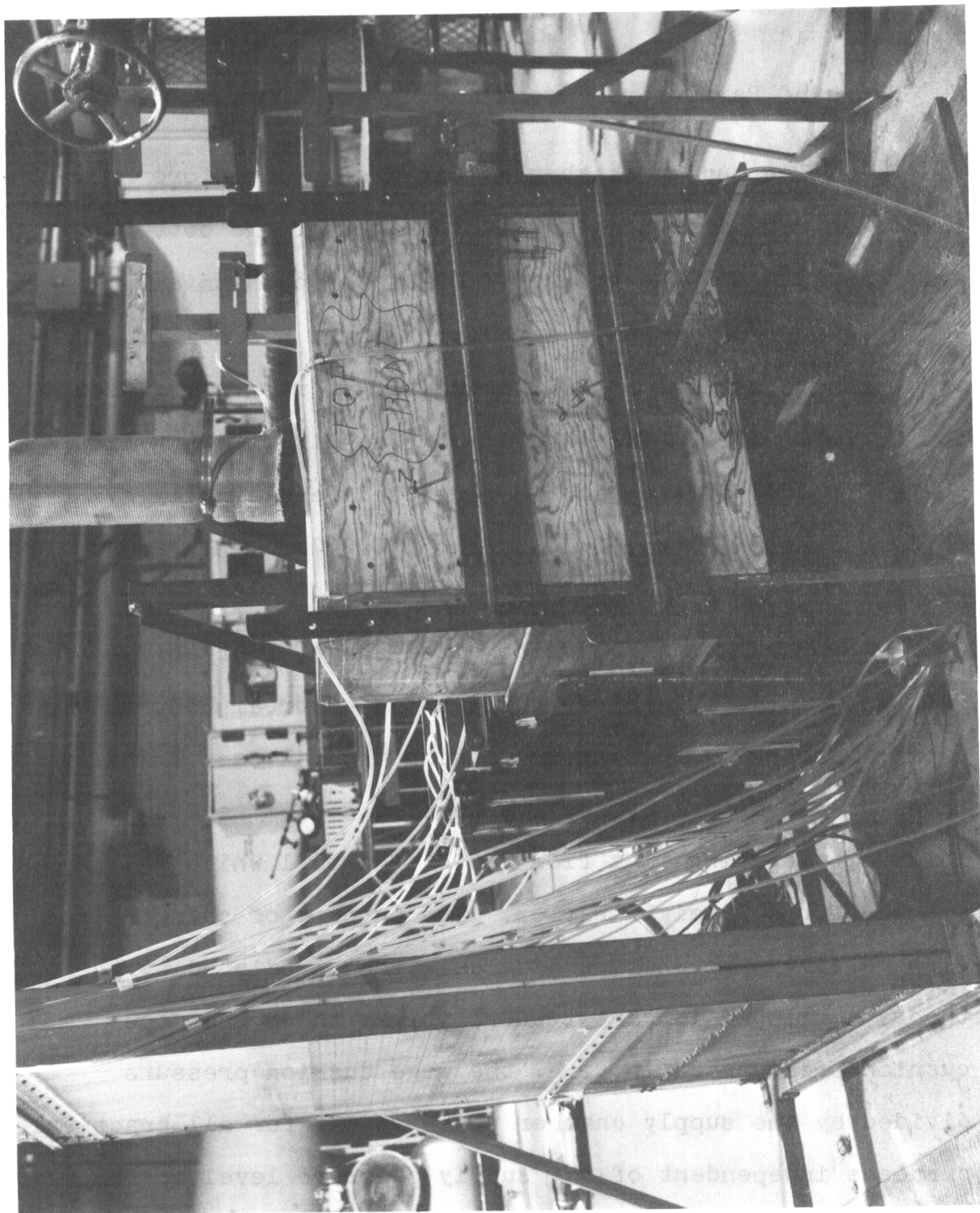
Figure 8   Frontal View of Test Assembly

e. Range of Parameters Investigated

      The supply chamber as was discussed before had a
sliding arrangement such that the height of the bottom
orifice plate and the ground floor of the cushion air chamber
could be varied. In this experiment work, the height, i.e.
the ground clearance in ACLS terminology, was varied from
0.5 to 7.5 inches. The flow length was fixed at $L = 12"$ and
the six values of clearance H were used resulting in six
(H/L) values of 0.064, 0.101, 0.165, 0.267, 0.437, and
0.603.

      For each (H/L) value cited above, four or five
flow rates were maintained through the upstream control
piping network by opening or closing the valves. The flow
rates ranged from a typical value of 0.36 lbm/sec to 1.6
lbm/sec, resulting in a flow ratio of 4 to 1 which was the
average for all height ratios. The purpose of changing the
flow rates was to check the calculations predicted by the
theory developed in Part I where it was shown that the
cushion pressure ratio, i.e. the gage cushion pressure
divided by the supply chamber pressure was for all practical
purposes independent of the supply pressure level or the
flow rates. For each height ratio, five flow rates were used.
For each orifice plate, six height ratios were used and three
orifice plates were employed so that altogether ninety-odd
runs were made.

f. Procedure

The locations of the pressure taps on the cushion
chamber surface are shown in Figure 5. The numbering system
for the pressure taps is also given in the figure. All of
the pressure taps used in the cushion chamber, except two,
were connected to the bank of water manometers as shown in
Figures 7 and 8. The other two taps which are tap 12 row 1
and tap 17 row 3 were connected to draft gages. These taps
were used to measure the pressure distribution on the ground
board under the multi-orifice plate and on the cushion
chamber surface. The pressures which were measured by taps
8-21 for all three rows were found to be very close (within
1 percent) at each tap and their average value was taken to
be the cushion pressure. The value of the cushion pressure
which was measured was usually very small (less than 0.50
inches of water) except at small values of the height ratio.
Since the water manometers used had a readability of at best
0.01 inches, draft gages were used to obtain a more accurate
value of the cushion pressure. By checking the readings
of the cushion pressure taps connected to the water manometer,
it was possible to see if the pressure on the surface of the
cushion chamber varied. While by using the cushion pressure
obtained from the draft gages, it was possible to obtain a
more accurate value of the cushion pressure.

At a given height ratio between three to nine different values of the mass flow rate were measured along with the cushion pressure and the supply total pressure. The mass flow rate was varied throughout the entire range of mass flow rates within the capability of the laboratory supply. However, this was not always the best procedure to use. At larger height ratios, the accuracy of the measurements taken at low mass flow rates was greatly reduced due to the small values of the total pressure and the cushion pressure distribution. This greatly affected the cushion pressure distribution readings since the cushion pressure distribution was being measured by the water manometers. Thus, in order to obtain a more accurate value of the cushion pressure distribution ratio, the pressure distribution was measured only at the larger mass flow rates for each height ratio. Pressure distribution data were taken for two to three mass flow rates in order to ascertain if the distribution ratio was affected by the mass flow rate. Because the readibility of the draft gage was of the order of 0.001 inch, the cushion pressure was maintained above 0.050 inch of water, in order to obtain accurate measurements.

The direction of the flow in the cushion chamber indicated from the visual observations of the tufts located throughout the chamber was recorded only once at each height ratio since the direction of the flow did not appear to fluctuate for different mass flow rates.

It was desirable to obtain a uniform total pressure distribution across the width (no-flow direction) of the supply chamber in order to simulate a two-dimensional flow pattern. The variation of the total pressure in the no-flow direction was determined from the cushion pressure distribution data. This was because the major cause of a cushion pressure variation in the no-flow direction was due to the total pressure variation in the supply chamber in that direction. At large height ratios, however, the side walls of the cushion chamber also contributed to a cushion pressure variation in the no-flow direction which made it difficult to determine the total pressure variation.

Total pressure variation data were taken across the supply chamber by traversing in the main-flow direction in order to record the maximum total pressure. The maximum total pressure was used in the calculations of the cushion pressure ratio, flow, the discharge coefficient, and the cushion pressure distribution ratio in order to simplify the data reduction.

Throughout the experiment, the pressure drop across the metering orifice was kept within the range of the mercury manometer since it was found that this procedure coincidentally produced a cushion pressure within the range of the draft gage. However, at the lower height ratios a pressure drop within the water manometer range provided the desired cushion pressure.

21

Once a desired cushion pressure was obtained and the flow had stabilized (when one of the flow valves was opened or closed, it usually took a few seconds for the flow to reach a new equilibrium), the metering orifice pressure drop, the air temperature, and the ambient temperature were recorded. Throughout the test the orifice pressure drop was checked to make sure that it had not varied. If the pressure drop had changed by over two percent, the test was rerun. The average values at the beginning and the end data were taken as the data to be used for the calculation of the mass flow rate.

For a height ratio greater than 0.620, the cushion pressure (due to the limitation of the laboratory air supply) was found to be too small to be read accurately by a manometer. Accordingly, 0.620 was chosen to be the upper limit although a greater value could be achieved from a geometrical viewpoint. At this height ratio, the maximum cushion pressure was about 0.10 inch of water. On the other hand, a minimum height ratio of about 0.05 was chosen since it was difficult to adjust and align the supply chamber below this value. These values also provided the range over which it was desired to vary the height ratio. Intermediate values of the height ratio were chosen so that a smooth curve could be obtained when the data were plotted. The height ratio was measured with a steel rule

at three points across the front of the cushion chamber, and the average of those three readings was reported. (The variation was less than 0.02 inch.) A small carpenter's level was used to make sure that the supply chamber was level horizontally and true vertically relative to the ground board of the cushion chamber.

Velocity profile data were taken at the exit of the cushion chamber for two height ratios of about 0.6 and 0.2 in order to determine the effect of the height ratio on the flow distribution. The profile was taken at the center of the cushion chamber exit in order to minimize the effects of the cushion side walls. A Pitot-static tube (one-eighth of an inch in outer diameter) was used, and the pressure differential was measured on the draft gage. The Pitot tube was mounted to a ring-stand by means of a ring-stand clamp. The height of the Pitot tube was measured by a steel rule. The profile was taken at a large mass flow rate so that the pressure differential was larger and could be measured more accurately than at a lower flow. Also, the velocity profile was integrated to yield an average velocity which was compared to the average velocity obtained by dividing the mass flow rate by the density of the air and the exit area.

IV. RESULTS

In this experimental work each test run was made with fixed values of the following parameters:

(1) The area ratio A_r of air injection area to the total plate area. This was determined by the orifice plate used and ranged from 0.06 to 0.18 (see Table 1).

(2) The height ratio (H/L) of the clearance H to the flow length L. This ratio ranged from 0.06 to 0.6. The latter was controlled by the laboratory air supply; beyond this value of 0.6 the cushion pressure became too small to be measured accurately.

(3) The supply chamber total pressure p_t or the trunk pressure. This value was adjusted by controlling the upstream valve settings, limited by the laboratory air capacity.

For these parametric values, the actual data taken were as follows:

(1) The gage pressure readings of the pressure taps No. 1 through 21. Taps No. 1 through 7 were located directly below the orifice discharge plate attached to the bottom of the supply chamber. Taps No. 8 through 21

were located on the periphery of the cushion
chamber (see Figure 5 for dimensions).

(2) The pressure readings of the flange taps
     upstream and downstream of the metering
     orifice plate in the upstream pipe circuit.
     This orifice assembly was constructed
     according to the ASME standards and the
     orifice coefficients were known to be
     within 1.0%.

(3) The velocity-head at the exit section of
     the cushion air passage. This served to
     indicate the profiles as actually obtained
     versus those predicted by the theory in
     Part I.

(4) The total pressure survey in the supply
     chamber. This was for the purpose of
     identifying any serious non-uniform distri-
     bution of the total pressure in the supply
     chamber (trunk) either attributable to the
     effect of the inlet to the supply or to the
     effect of the exit (orifice discharge)
     from the chamber. It was found that for
     larger height ratio there was more non-
     uniformity to the total pressure in the
     supply chamber than for smaller height ratio.

This effect was discussed in Appendix II.

In making detailed computations, however, the maximum value among the total pressure variation was used as the supply chamber total pressure.

Altogether three orifice plates were used to simulate the orifice pattern on the cushion bag during the stiff-mode operation. These orifice plates had area ratios A_r of 0.06, 0.112, and 0.18 respectively. The discharge coefficients C_d for these orifice plates were determined in a separate calibration work to be discussed in Appendix I.

For each orifice plate used, six or seven height ratios (H/L) were attained. The largest ratio was 0.6 and was, as mentioned before, controlled by the measurability and accuracy of the cushion pressure. The lowest ratio of 0.06 was governed by the alignment problem between the ground board (floor) and the cushion bottom (orifice-plate). For each setting of the (H/L)-valve, four or five different flow rates corresponding to four or five supply chamber pressures were maintained. The range of flow rates was about four to one (4:1). The number of test runs was therefore about 4 x 6 x 5 = 120 runs. The data taken were listed and tabulated in various graphs and tables to be discussed in the following.

a. Cushion Pressure Ratio

The cushion chamber wall pressure as indicated
by taps 8-21 was found to be essentially independent of
position. Although some fluctuations in these cushion
pressure readings were observed, the variation on a gage-
basis was on the order of less than two percent or about
0.02 inches of water. The minute variation of the pressure
tap readings from No. 8 through 21, i.e., around the
periphery of the cushion space can be judged from Table 2.
At low height ratios the variation was on the order of
two percent and increased to six percent at $H/L = 0.6$.
This observation tends to support the assumption used in
the theory of Part I that the cushion air space in stiff-
mode operation contained negligible air motion. However,
the thread tufts located on the cushion chamber wall did
indicate a circulatory motion which was of negligible
influence at lower height ratio but was of an appreciable
magnitude to cause a discernable deviation of the theore-
tical results from the experimental data.

The cushion pressure ratio defined as the gage
pressure in the cushion space (average reading of taps 8-21)
divided by the supply chamber gage pressure were found to
be virtually independent of the flow rates through the
discharge orifice plate at the supply-chamber bottom.

27

TABLE 2

Cushion Chamber Pressure and Peripheral Variations

A_r	H/L	P_t in. H_2O Gage	P_c in. H_2O Gage	P_c/P_t cushion Pr. ratio	P_c Variation in. H_2O (%)
0.180	.064	1.506	1.470	0.976	.02 (1.3)
		2.240	2.200	0.956	.06 (2.7)
		2.94	2.87	0.977	.01 (0.3)
	.101	1.180	1.035	0.878	.03 (2.9)
		1.475	1.280	0.868	.02 (1.6)
		2.175	1.880	0.865	.04 (2.1)
	.165	0.815	0.480	0.581	.01 (2.1)
		1.220	0.720	0.590	.01 (1.4)
	.267	0.890	0.320	0.359	.01 (3.1)
	.436	0.740	0.160	0.216	.01 (6.3)
0.112	.052	2.090	1.975	0.945	.01 (0.5)
		3.53	3.27	0.927	.02 (0.6)
		4.65	4.39	0.944	.02 (0.5)
	.274	1.865	0.310	0.167	.01 (3.2)
0.060	.064	2.145	0.760	0.354	.01 (1.3)
		5.46	1.940	0.355	.04 (2.1)
		7.25	2.50	0.345	.06 (2.4)
	.108	9.79	2.000	0.204	.02 (1.0)
	.454	8.71	0.170	0.195	.01 (5.9)

Although there were some fluctuations among the data at different flow rates, these fluctuations were quite random and small and did not exhibit any rational trend. There were, however, greater fluctuations from their mean value at the lower flow rates. This is believed to be caused by the less accurate measurements of the pressure readings of the manometers.

The overall performance of the ACLS at the stiff-mode operation is of course indicated by the cushion pressure ratios. Table 3 lists the experimental values of the cushion pressure ratios for various parametric conditions noted thereon. A very significant observation is that the pressure (cushion) ratio remained almost constant while the flow rate varied threefold. The averaged cushion pressure ratios were tabulated in Table 4 together with those computed from the theory. The experimentally obtained ratios were found to be dependent upon the orifice-plate used and the height ratio (H/L). The former was characterized by the product of the area ratio A_r and the discharge coefficient C_d of the orifice assembly. The discharge coefficients based on the data (see Figure 39) from Appendix I were found to be 0.615, 0.608, and 0.605 for orifice plates No. 1, 2, and 3 with A_r = 0.18, 0.12, and 0.060 respectively. This characterization parameter was deduced in Part I (Theory). In order to

29

Table 3

Pressure Ratio, Mass Flow Versus Height Ratios

(For $A_r = 0.18$)

H/L	P_c in H_2O gage	P_t in H_2O gage	$(P_c/P_t)_{gage}$	Flow lb/sec
0.603	0.065	0.492	.132	1.323
	0.085	0.660	.129	1.569
	0.095	0.705	.134	1.643
0.436	0.040	0.175	.229	0.813
	0.058	0.265	.219	0.956
	0.080	0.400	.200	1.203
	0.105	0.485	.217	1.315
	0.160	0.740	.216	1.617
	0.160	0.750	.213	1.637
0.267	0.055	0.150	.367	0.691
	0.110	0.310	.354	0.957
	0.178	0.480	.371	1.186
	0.170	0.470	.362	1.206
	0.200	0.545	.367	1.275
	0.315	0.900	.350	1.611
	0.320	0.890	.360	1.635
0.165	0.075	0.120	.625	0.526
	0.085	0.140	.607	0.553
	0.400	0.670	.597	1.224
	0.480	0.815	.589	1.318
	0.690	1.180	.584	1.596
	0.720	1.220	.590	1.620
0.101	0.080	0.090	.889	0.355
	0.780	0.885	.881	1.038
	1.035	1.180	.877	1.159
	1.210	1.385	.874	1.275
	1.280	1.475	.868	1.326
	1.880	2.175	.864	1.601
0.064	.620	0.630	.984	0.572
	1.350	1.370	.985	0.864
	1.470	1.506	.976	0.893
	2.200	2.240	.982	1.076
	2.87	2.94	.976	1.241

Table 3 (CONT'D)

(For $A_r = 0.112$)

H/L	P_c in H_2O gage	P_t in H_2O gage	$(P_c/P_t)_{gage}$	Flow lb/sec
0.608	0.025	0.410	.061	0.845
	0.095	1.600	.059	1.592
	0.098	1.650	.059	1.619
0.440	0.075	0.835	.090	1.132
	0.093	1.025	.091	1.245
	0.150	1.665	.090	1.607
	0.160	1.750	.091	1.638
0.274	0.093	0.505	.184	0.872
	0.090	0.555	.162	0.900
	0.150	0.930	.161	1.145
	0.183	1.065	.172	1.236
	0.220	1.265	.174	1.327
	0.310	1.865	.166	1.583
	0.320	1.930	.166	1.635
	0.333	1.985	.168	1.657
0.172	0.090	0.280	.321	0.608
	0.165	0.505	.327	0.812
	0.330	1.010	.327	1.117
	0.390	1.225	.318	1.238
	0.500	1.605	.312	1.392
	0.680	2.230	.304	1.638
0.107	0.080	0.138	.580	0.378
	0.300	0.510	.588	0.691
	0.540	0.905	.597	0.907
	0.848	1.470	.577	1.137
	1.030	1.748	.589	1.232
	1.220	2.120	.576	1.358
0.052	0.100	0.105	.952	0.181
	0.325	0.340	.956	0.327
	0.370	0.395	.937	0.345
	0.543	0.582	.933	0.423
	0.870	0.925	.941	0.526
	1.975	2.090	.945	0.806
	3.27	3.53	.926	1.065
	4.39	4.65	.944	1.221

Table 3 (CONT'D)

(For $A_r = 0.060$)

H/L	P_c in H_2O gage	P_t in H_2O gage	$(P_c/P_t)_{gage}$	Flow lb/sec
0.620	0.040	3.21	.013	0.994
	0.060	4.28	.014	1.145
	0.080	6.01	.013	1.360
	0.100	7.72	.013	1.558
0.454	0.047	2.33	.020	0.832
	0.085	4.29	.020	1.153
	0.097	4.76	.020	1.217
	0.165	8.45	.020	1.626
	0.170	8.71	.020	1.639
0.286	0.063	1.620	.039	0.699
	0.098	2.57	.038	0.879
	0.170	4.69	.036	1.159
	0.200	5.25	.038	1.234
	0.335	8.91	.038	1.620
0.180	0.100	1.600	.063	0.671
	0.205	3.33	.062	0.958
	0.370	5.81	.064	1.260
	0.490	7.58	.064	1.469
	0.600	9.23	.065	1.616
0.108	0.110	0.535	.206	0.383
	0.260	1.295	.201	0.584
	0.330	1.640	.201	0.662
	0.450	2.320	.194	0.783
	1.030	5.00	.206	1.139
	2.000	9.79	.204	1.598
0.064	0.100	0.265	.377	0.243
	0.245	0.685	.358	0.399
	0.500	1.395	.358	0.571
	0.760	2.145	.354	0.708
	1.940	5.46	.355	1.158
	2.50	7.25	.344	1.322
0.046	0.105	0.145	.724	0.143
	0.350	0.530	.660	0.289
	0.510	0.740	.689	0.351
	0.990	1.430	.692	0.477
	1.480	2.140	.692	0.610
	2.86	4.32	.662	0.875

Table 4

Theoretical Versus Experimental Results
Cushion Pressure Ratio

Area Ratio (Disch. Coef.)	Height Ratio H/L	Cushion Pressure Ratio $(P_c/P_t)_{gage}$	
		Experiment	Theory
0.180 (0.625)	.603	.132	.080
	.436	.216	.146
	.267	.362	.334
	.165	.599	.623
	.101	.876	.886
	.064	.981	.984
0.112 (0.608)	.608	.060	.031
	.440	.091	.059
	.274	.169	.143
	.172	.318	.314
	.107	.584	.594
	.052	.942	.943
0.060 (0.605)	.620	.013	.009
	.454	.020	.016
	.286	.038	.040
	.180	.064	.097
	.108	.202	.241
	.064	.358	.521
	.046	.688	.729

33

compare the theoretical data against the experimental values, the computer program presented in Part I was used to generate three curves for $C_d A_r$ = 0.1124, 0.069 and 0.0369. The results of these computations were shown in Figure 9. The experimental values were shown on this figure for comparison. The agreement between the theory and experimental values is indeed very good except at larger height ratios where the discrepancy can be attributed to the following factors: (i) a strong recirculation in the cushion air space, (ii) the jets from discrete orifices do not form a uniform stream as was assumed in the analysis of Part I, and (iii) entrainment effect from the ambient.

b. Air Pressure Distribution in Seal Channel

The air pressure on the ground board as measured by taps 1 through 7 was to indicate the pressure variation along the channel flow length. Located along the no-flow direction there were three rows of the taps 1-7 (see Figure 5). If the physical model were exactly two-dimensional these three rows of taps 1-7 would have identical readings. However, due to the side wall effect the total pressure in the supply chamber (trunk) had a variation of about 5% and the readings of the taps on these three rows showed a maximum variation of ten percent at the same length location but at different rows along the no-flow direction.
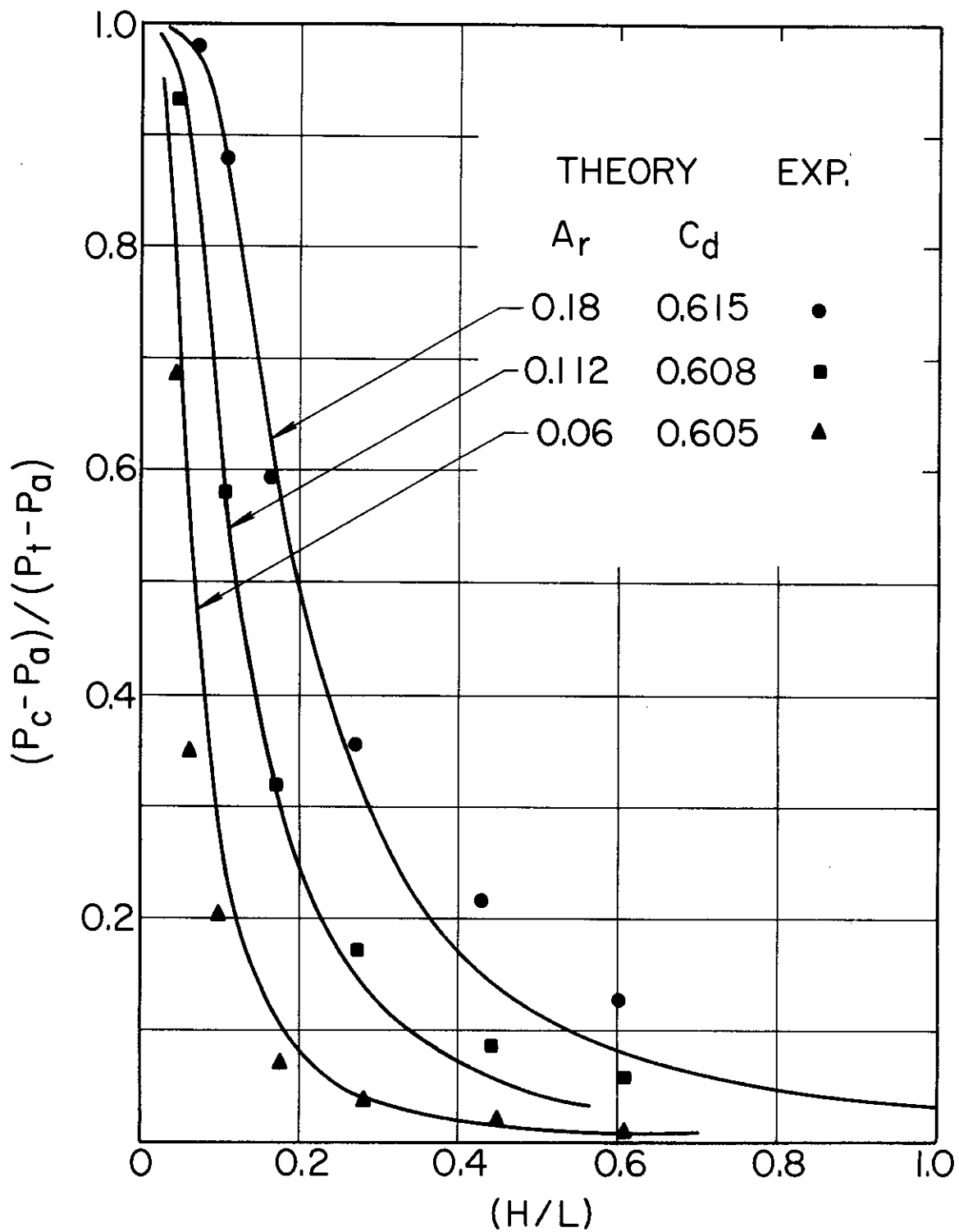
FIGURE 9   Cushion Pressure Ratio in
Stiff-Mode Operation

Figures 10 through 20 showed the variation of the pressure tap reading along the X-direction (main flow) as well as along the Z-direction. The arrangement of these figures showing the theoretical and experimental data are as follows:

Orifice-Plate No. 1 (A_r = 0.18) Figures 10-13,

Orifice-Plate No. 2 (A_r = 0.112) Figures 14-16,

Orifice-Plate No. 3 (A_r = 0.060) Figures 17-20 .

It appears reasonable to conclude that the variation of the pressure in the Z-direction is not significantly large. From these figures, it is apparent that the pressure distributions exhibited an increasingly pronounced peak which appears to be shifting outward as the value of (H/L) was increased, i.e. the height was increased. On these same figures were also shown the theoretical pressure ratio distributions computed from the theory developed in Part I. It can be concluded that the theory and experiments agreed on the main but there was an increasing divergence at larger height ratios at which the peaks in the experimental distribution curves became more prominent and shifted toward the exit. The same trend in the difference between the theoretical and experimental cushion pressure ratio was also observed as noted earlier.
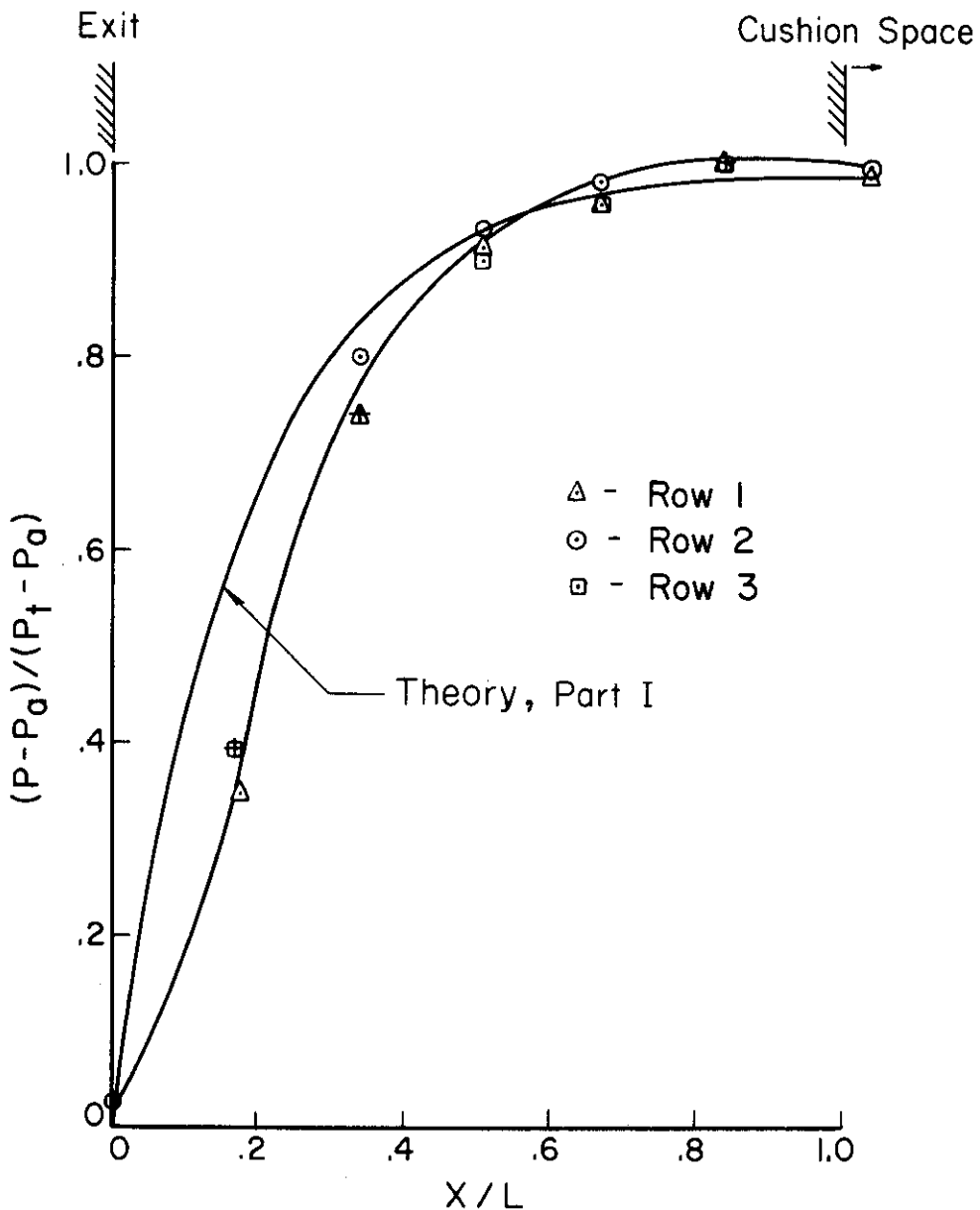
FIGURE 10. Pressure Distribution
in Ground Clearance
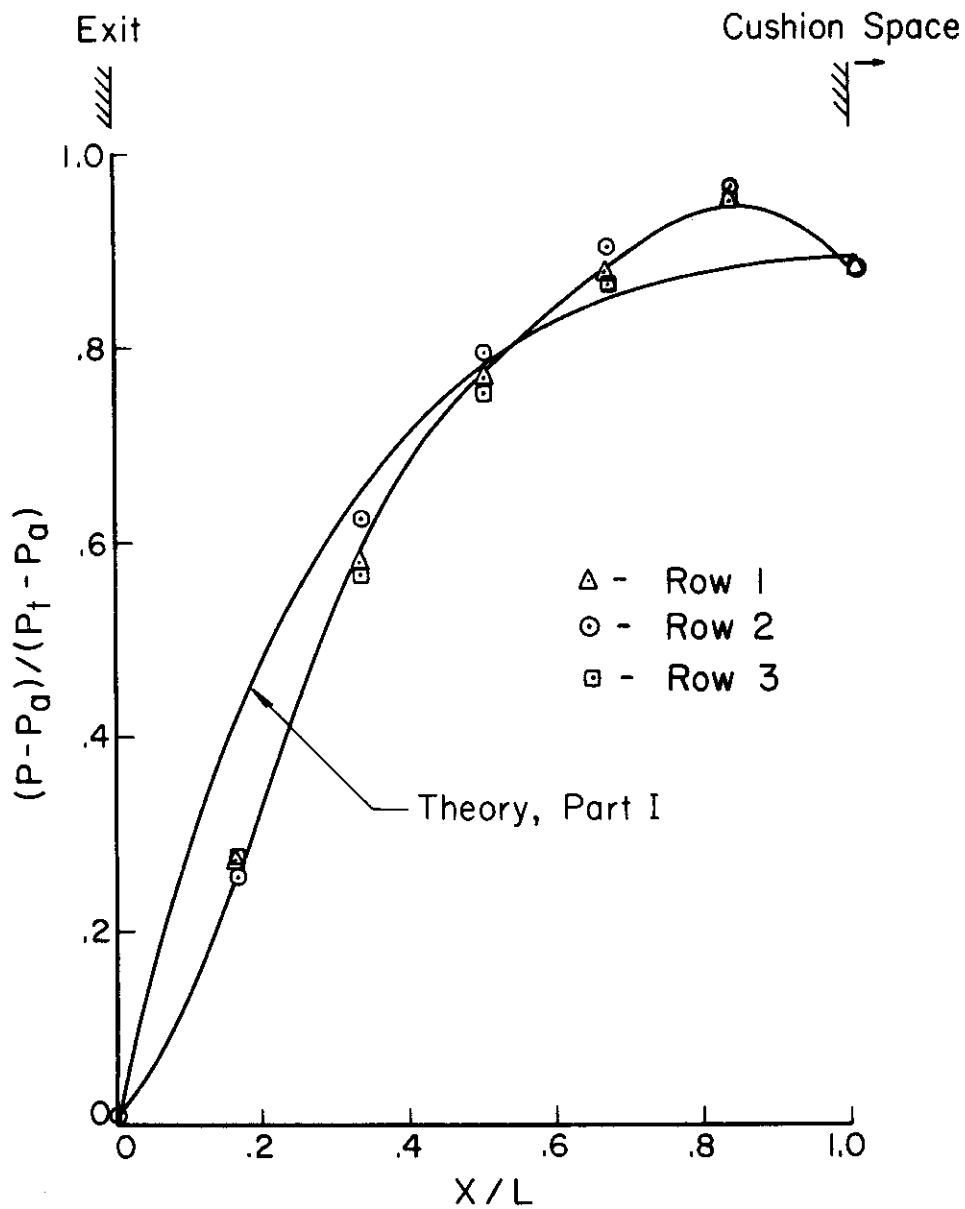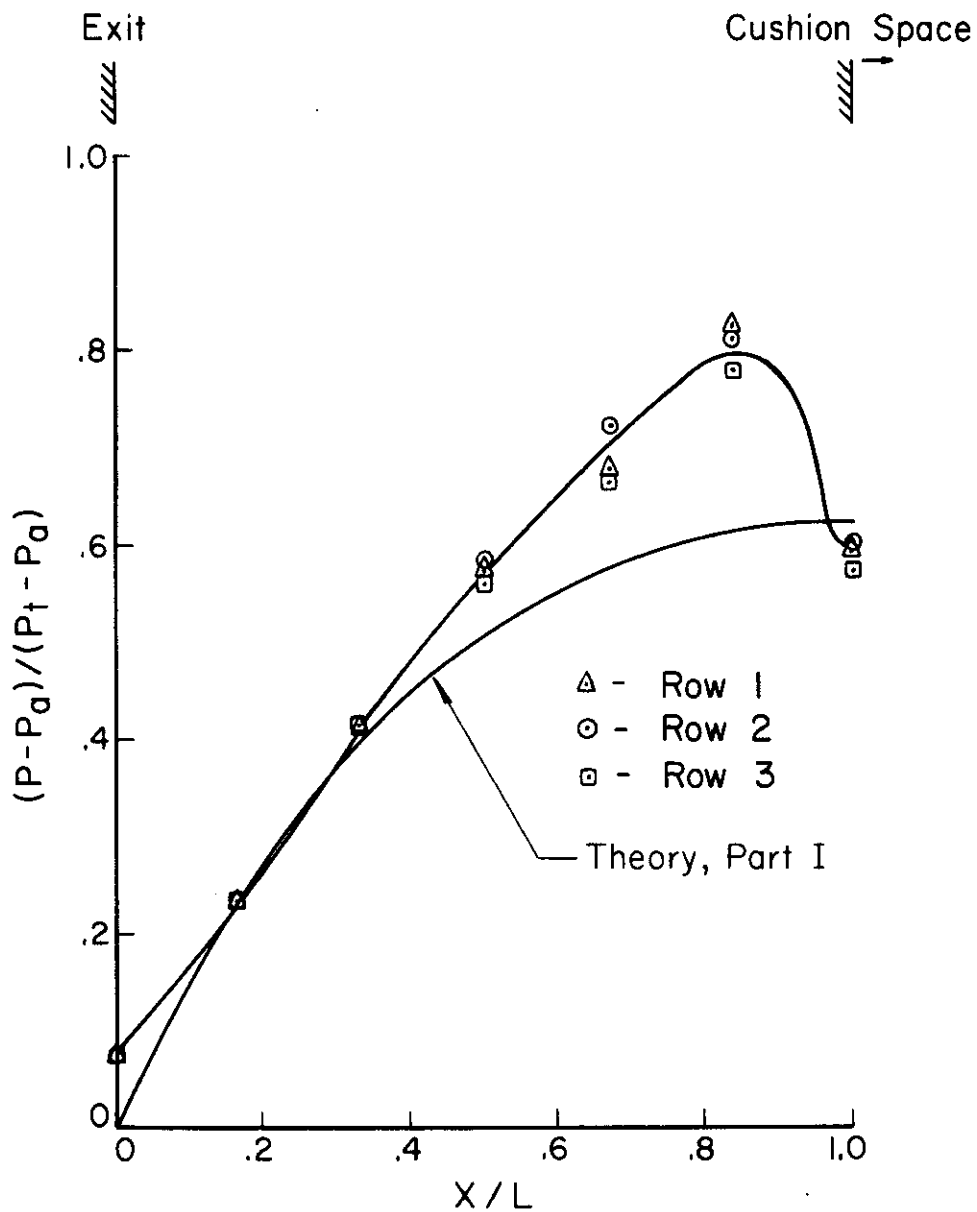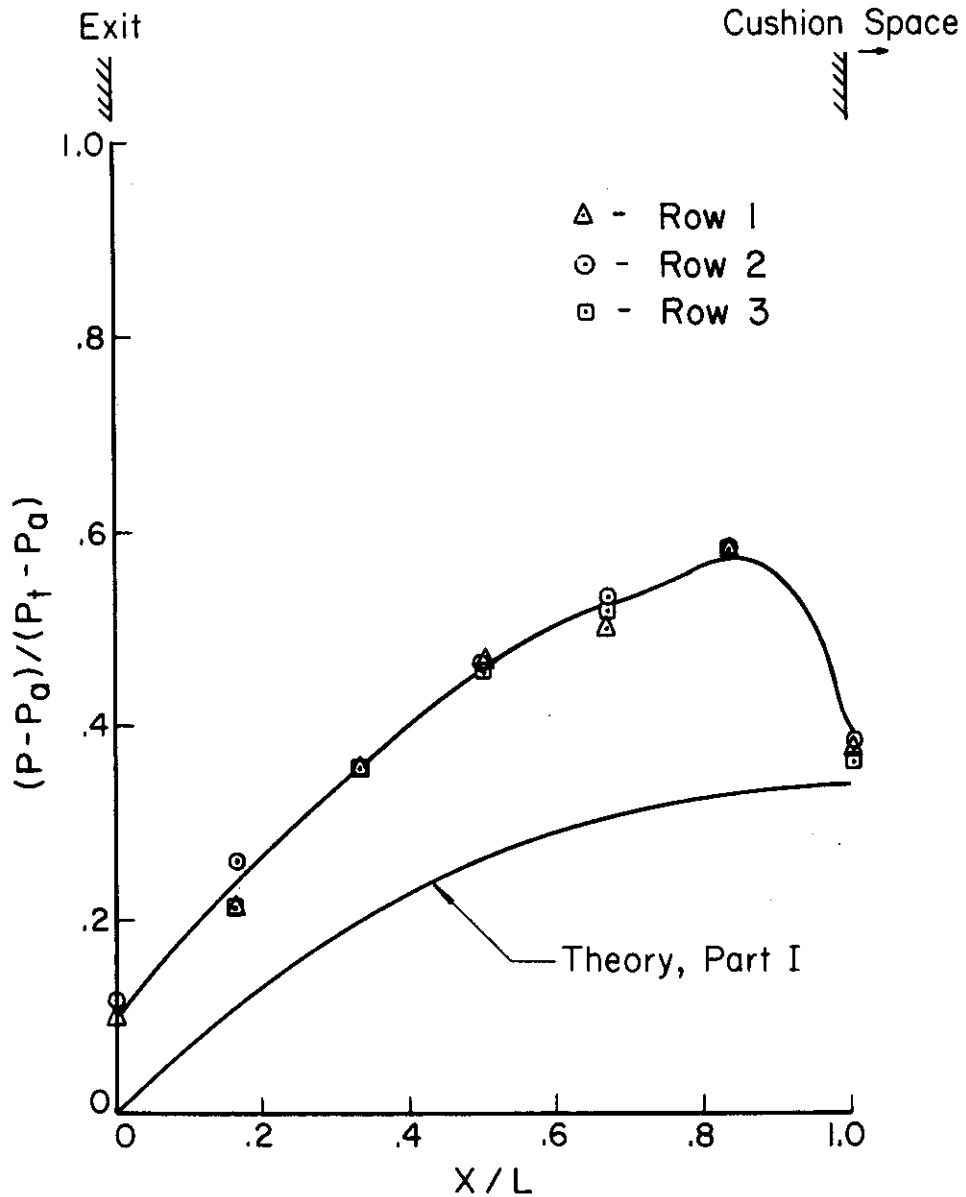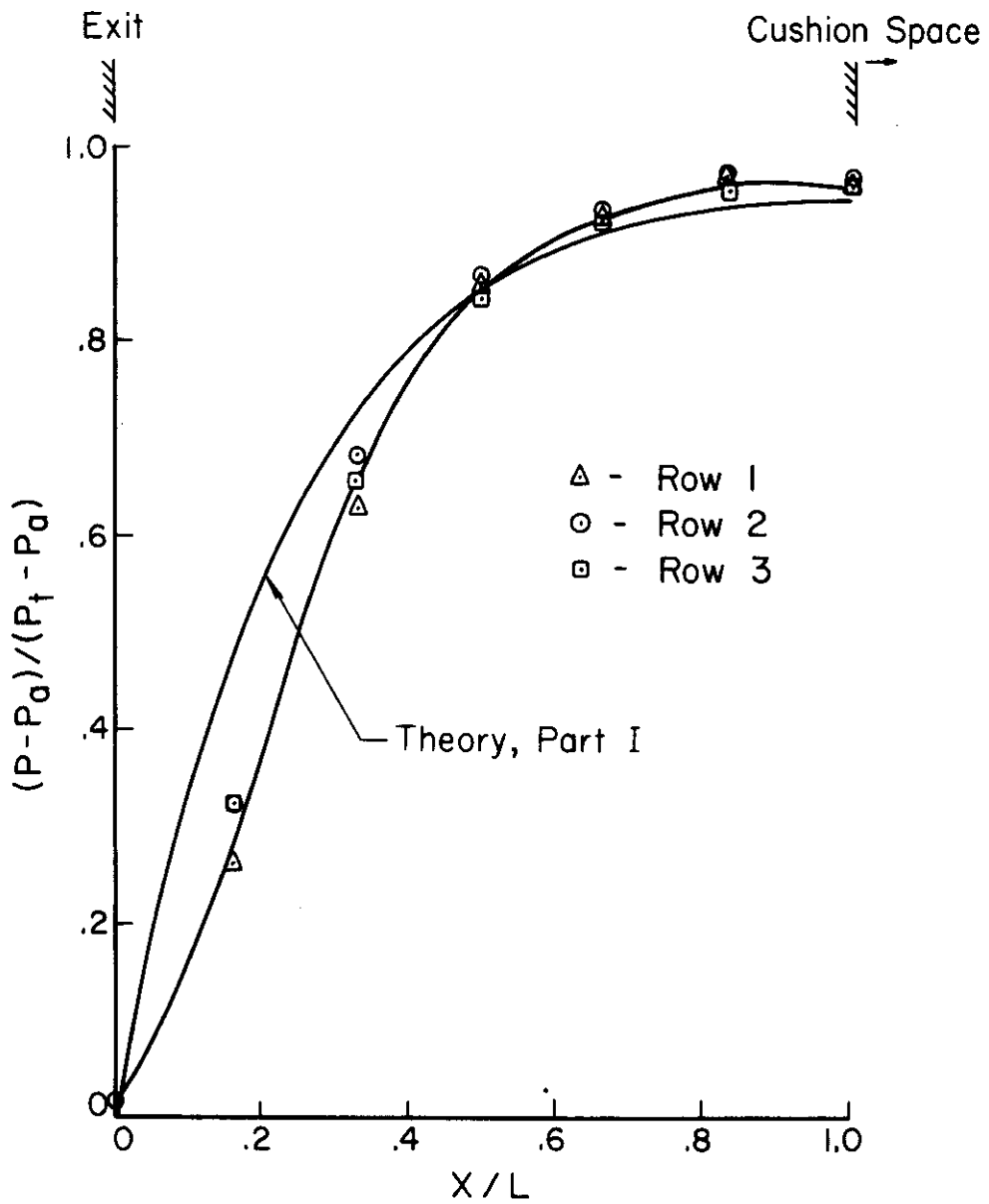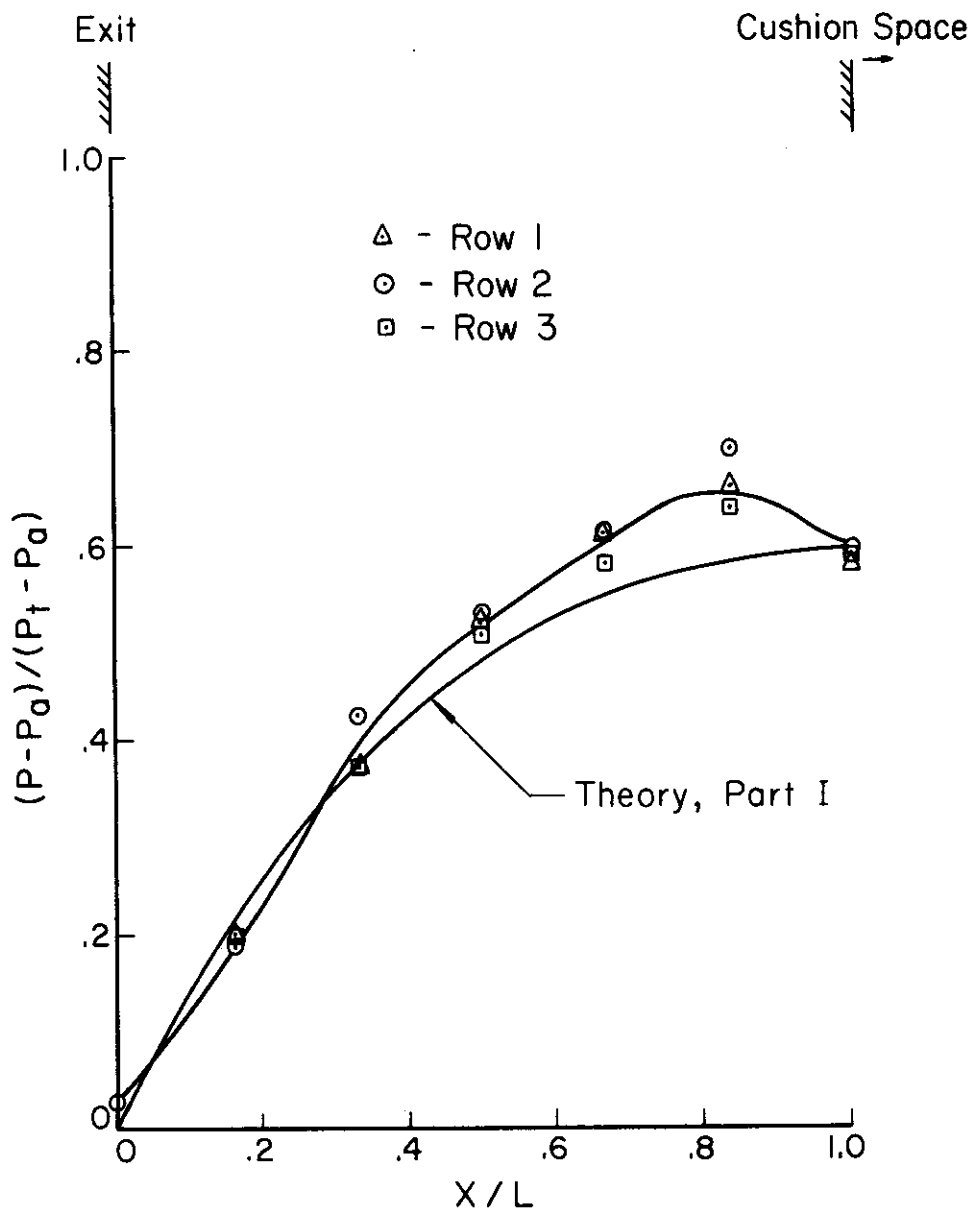$(A_r = .18, \quad H/L = .064)$

FIGURE 11.   Pressure Distribution
in Ground Clearance

$(A_r = .18, \quad H/L = .101)$

Exit

Cushion Space

FIGURE 12. Pressure Distribution
in Ground Clearance
$(A_r = .18 \quad H/L = .165)$

Exit Cushion Space

FIGURE 13.   Pressure Distribution
in Ground Clearance
$(A_r = .18, \quad H/L = .267)$

FIGURE 14.   Pressure Distribution
in Ground Clearance

$(A_r = .112, \quad H/L = .052)$

FIGURE 15.   Pressure Distribution
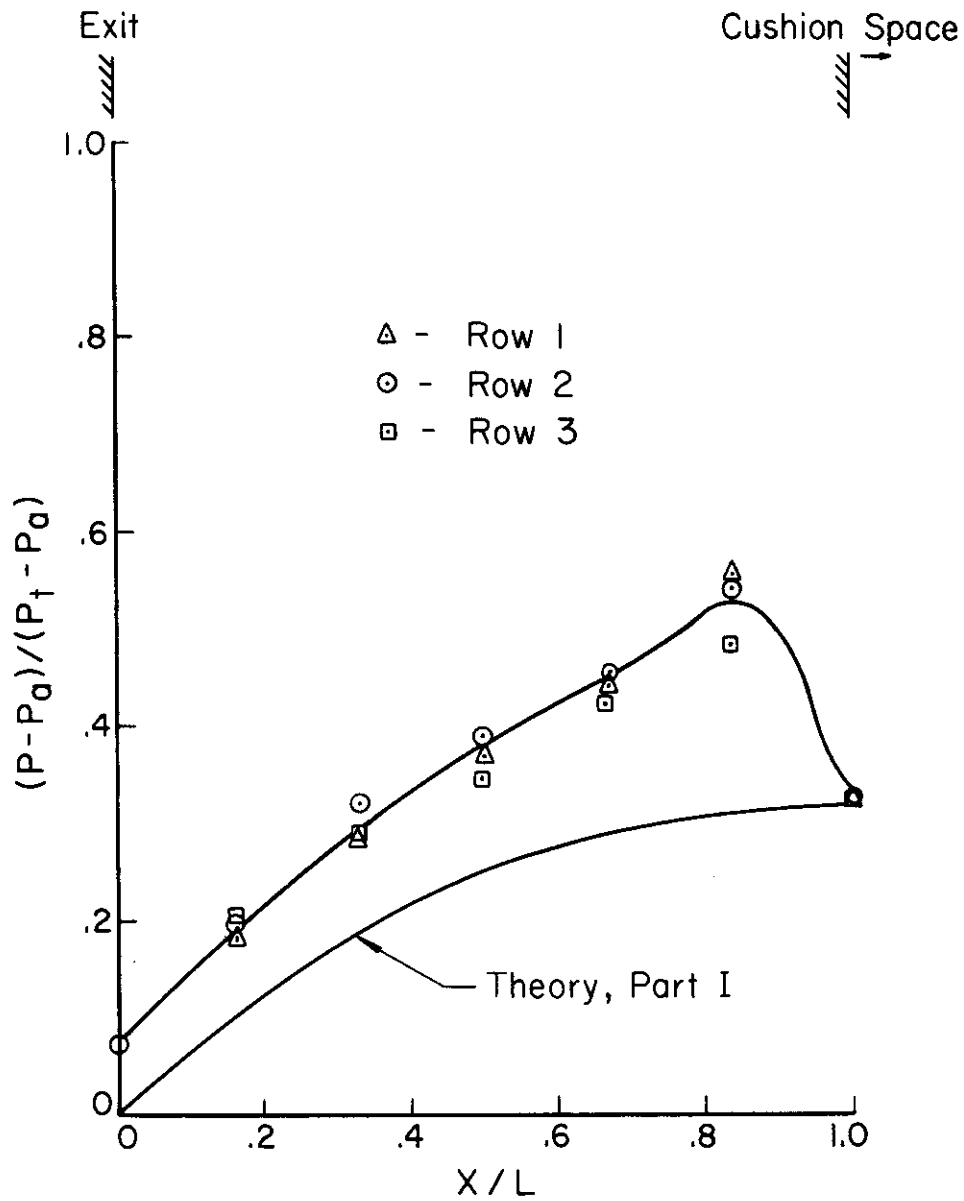in Ground Clearance
$(A_r = .112,   H/L = .102)$

FIGURE 16   Pressure Distribution
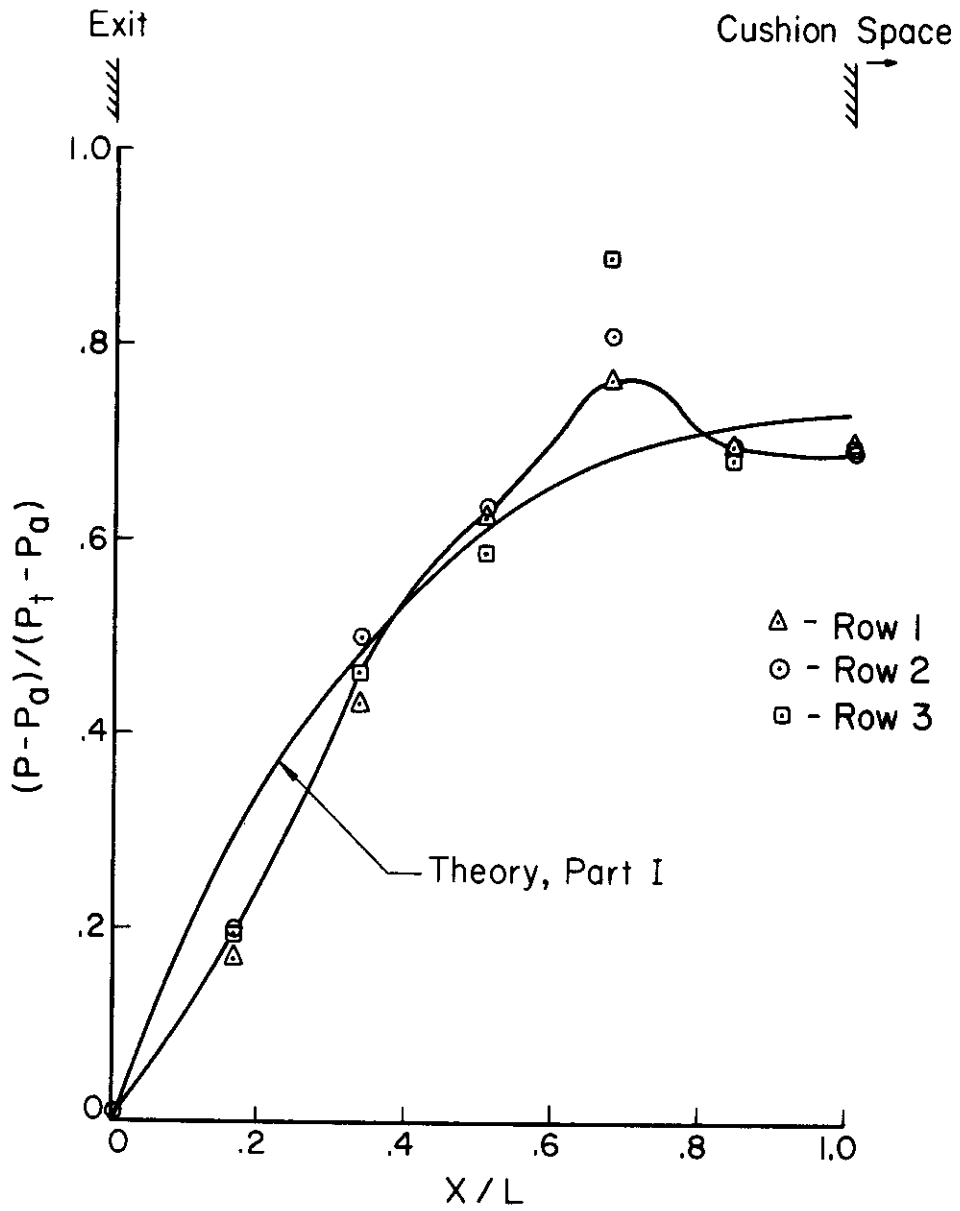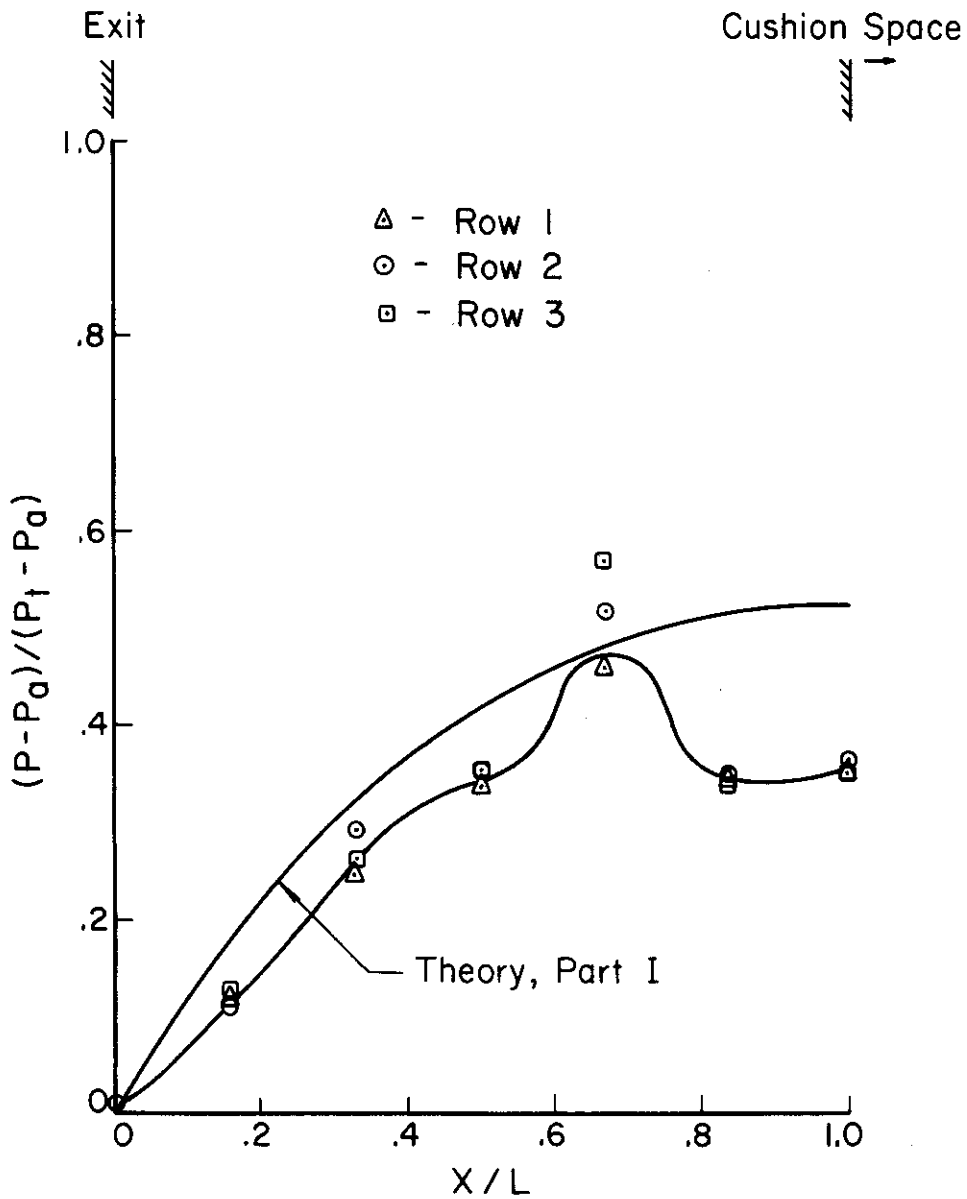in Ground Clearance
$(A_r = .112, \quad H/L = .172)$

FIGURE 17.   Pressure Distribution
in Ground Clearance

$(A_r = .060, H/L = .046)$

FIGURE 18   Pressure Distribution in Ground Clearance ($A_r = .060$, $H/L = .064$)
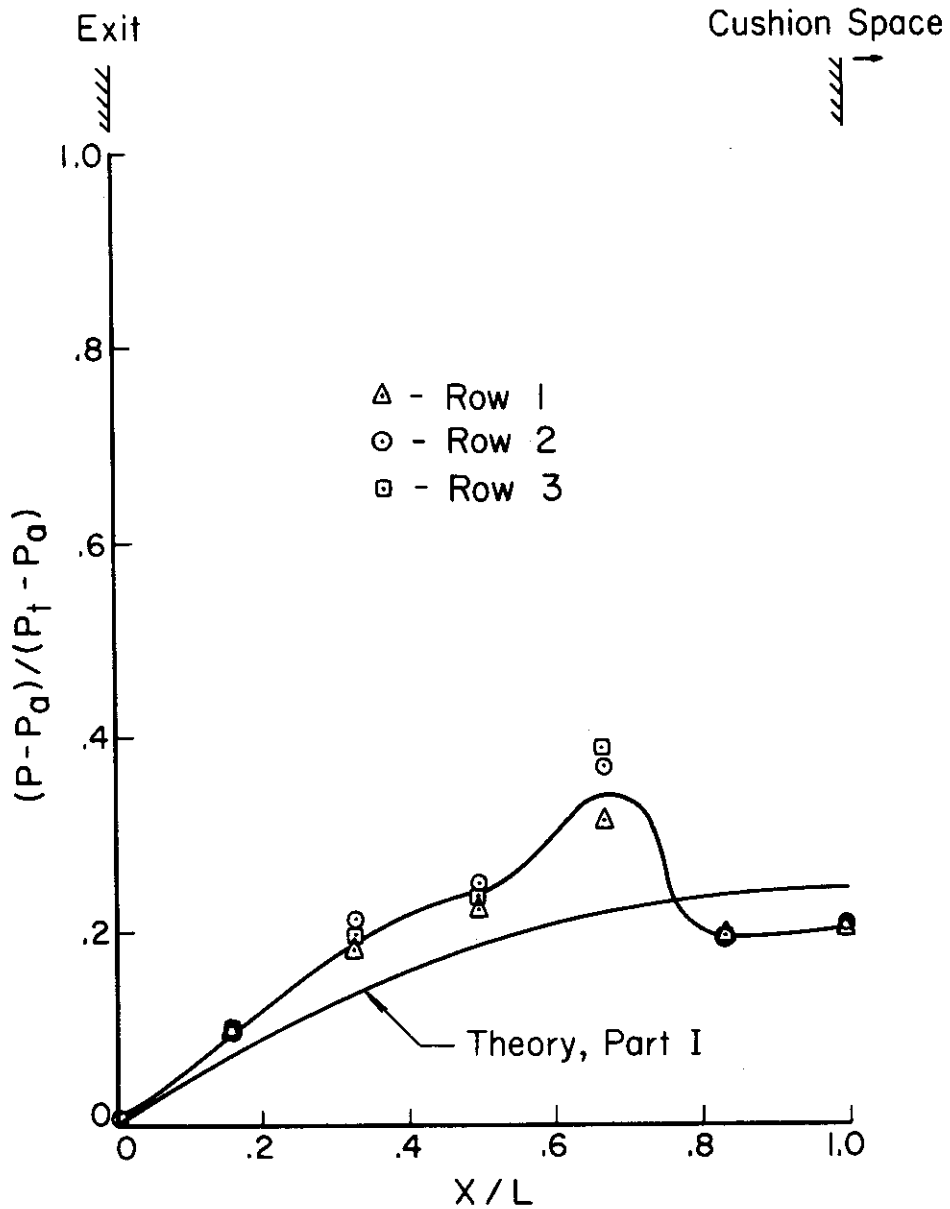
Exit

Cushion Space

$\triangle$ – Row 1
$\odot$ – Row 2
$\square$ – Row 3

Theory, Part I

$(P-P_a)/(P_t-P_a)$

X / L

FIGURE 19. Pressure Distribution
in Ground Clearance

$(A_r=.060, \ H/L=.108)$

Exit

Cushion Space

$\triangle$ – Row 1

$\odot$ – Row 2

$\square$ – Row 3

Theory, Part I

X / L
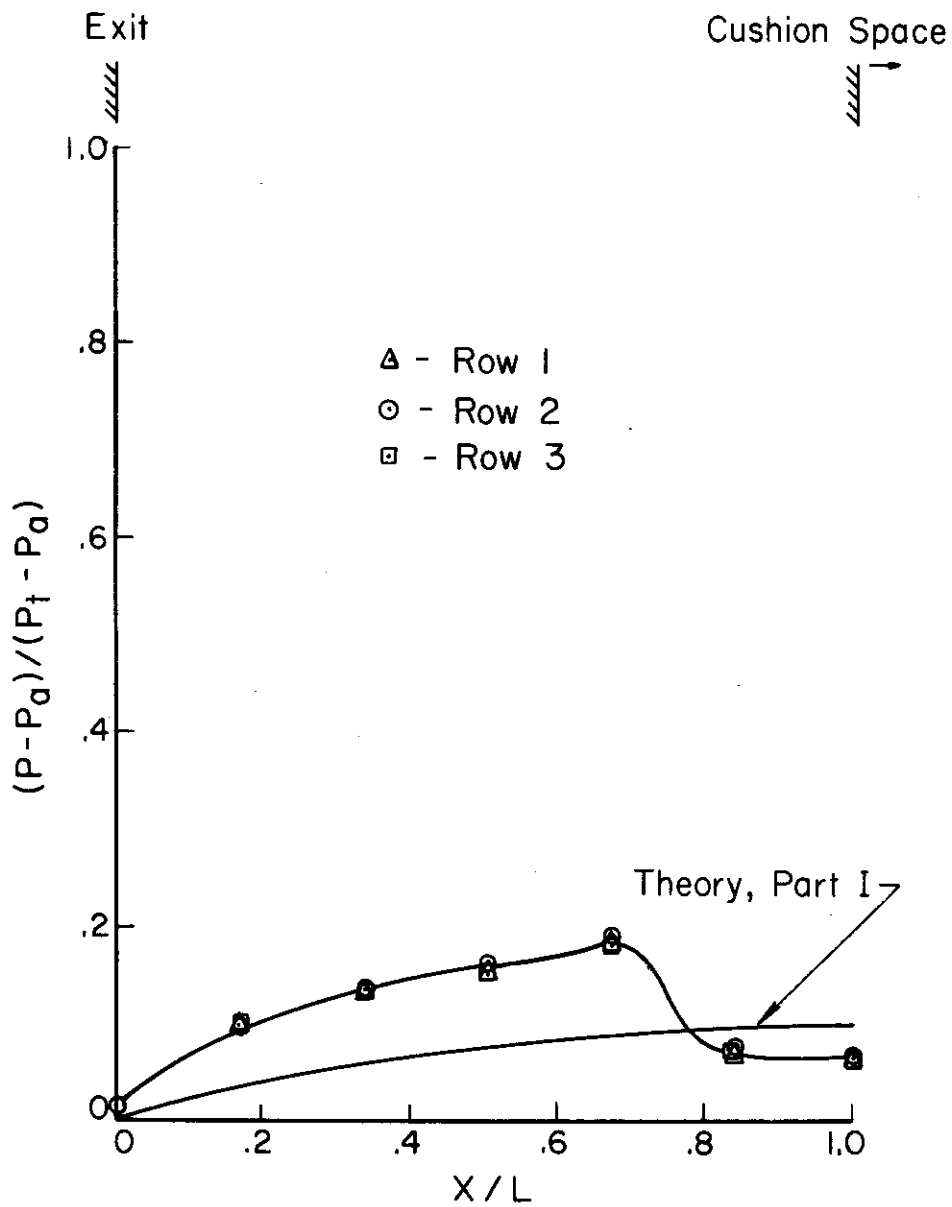
FIGURE 20. Pressure Distribution
in Ground Clearance

$(A_r = .060, \ H/L = .180)$

47

Figures 21, 22, and 23 are the summary plots, each for a fixed orifice plate, i.e. a fixed $C_d A_r$-value but with various height ratios. The existence of the peak pressure distribution as well as the increased discrepancy between theory and experiments can be attributed to the fact that at a larger height ratio, the cushion air after emerging from the discrete orifice holes formed a single merged jet rather than a continuous jet curtain spanning the entire orifice plate. From the local air flow direction data obtained by the thread tufts located on the walls the local flow direction near the pressure tap at which maximum pressure was recorded as to be outward from the cushion space. Figure 24 shows the tuft orientations during some typical test runs. Tap No. 7 was at the edge of the cushion space. Some side movements of air circulation were indicated. The bottom of Figure 24 showed the most abnormal motion. This appeared to be the dividing line. Furthermore, the lumped air jet did not, it was believed, occupy the entire flow channel while the air was being forced toward the exit. Such a plausible flow phenomenon was depicted in Figure 25.

That the flow channel at the exit section was not full was responsible for larger values of the measured cushion pressure ratio than those of the theoretical prediction.
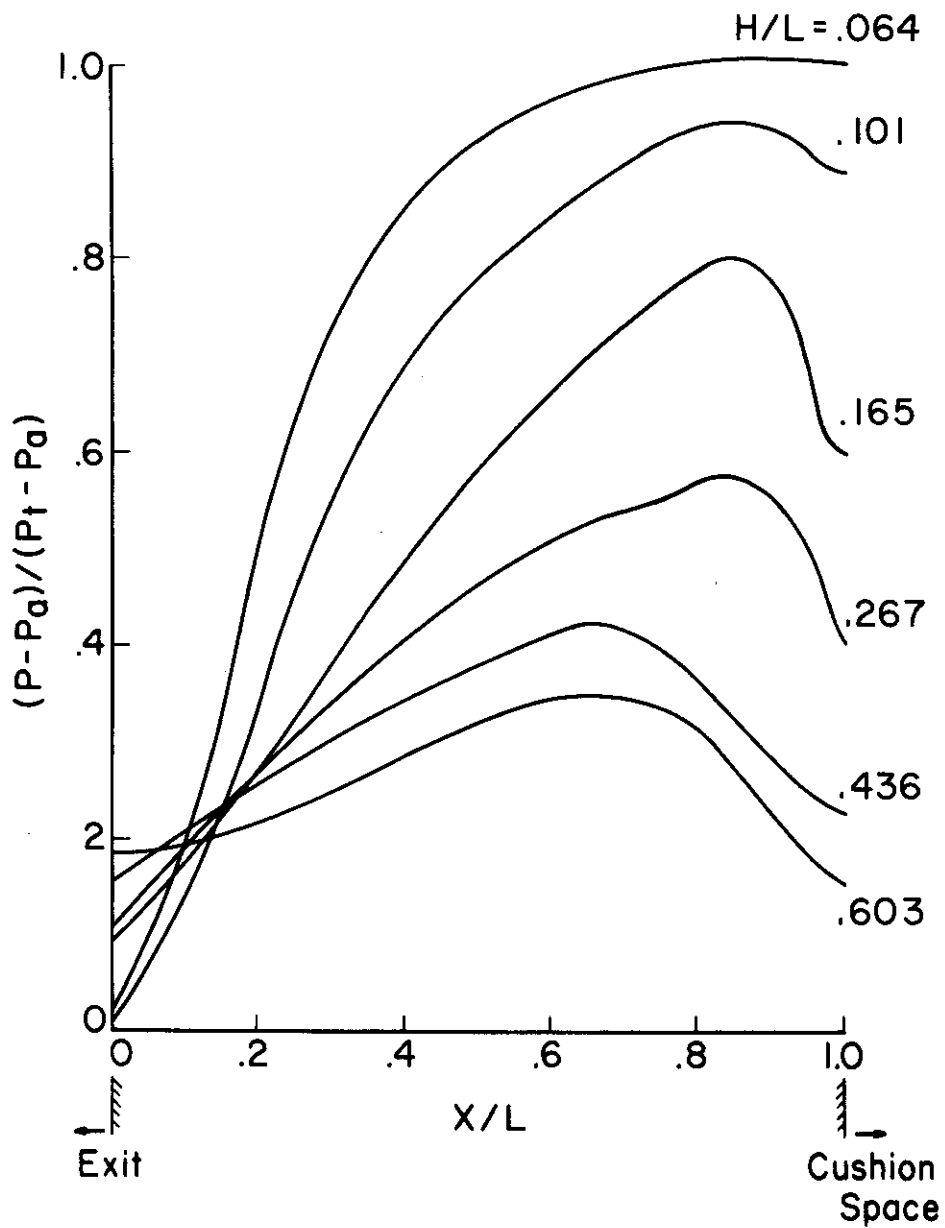
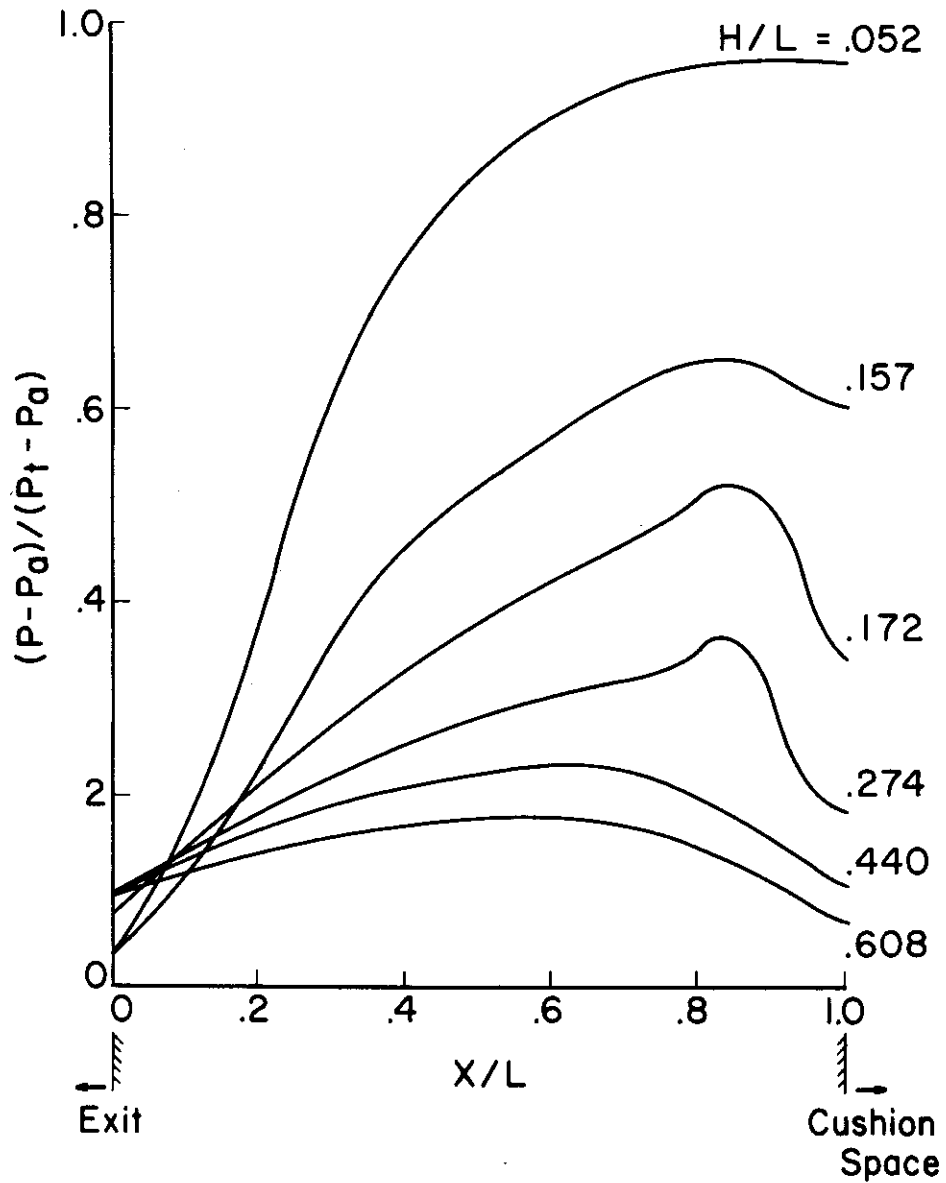FIGURE 21.   Pressure Distribution Ratio
in Cushion Chamber for Ar = 0.180

FIGURE 22.   Pressure Distribution Ratio
in Cushion Chamber for Ar = 0.120
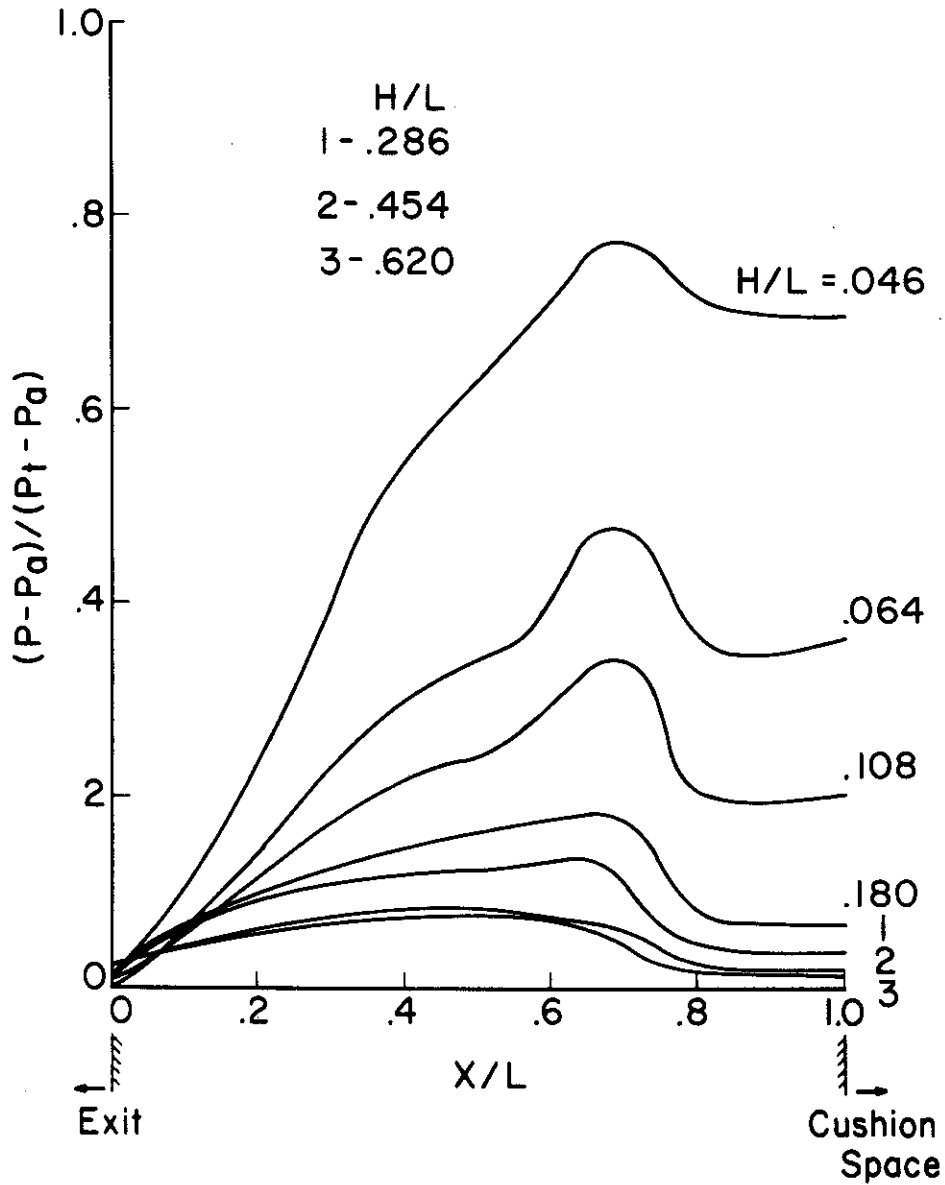
FIGURE 23. Pressure Distribution Ratio
in Cushion Chamber for Ar = 0.060

Graph labels:

Y-axis: $(P - P_a)/(P_t - P_a)$, values 1.0, .8, .6, .4, 2, 0

H/L
1 - .286
2 - .454
3 - .620

H/L = .046
.064
.108
.180
1
2
3

X/L

Exit
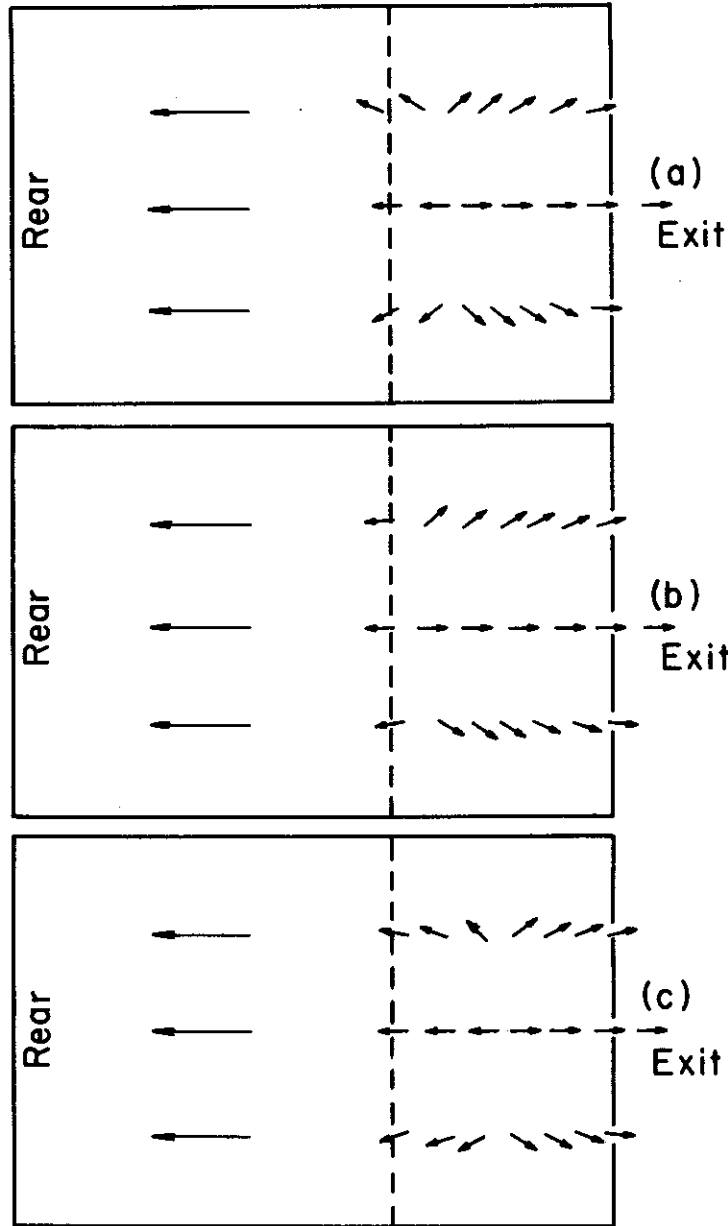
Cushion
Space

TOP VIEWS OF GROUND BOARD

FIGURE 24. Three Basic Flow Patterns Recorded on Ground Board of Cushion Chamber.
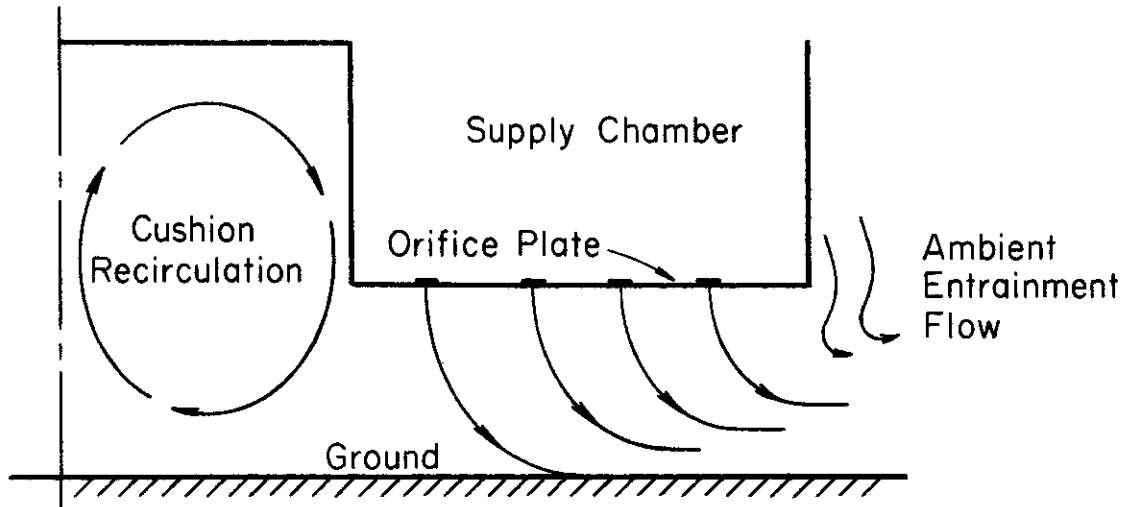
Figure 25. Entrainment Flow Pattern

This is so because for the same mass flow the reduced flow cross-section requires a greater velocity and hence greater momentum change and this in turn requires a greater cushion pressure than when the flow cross section at the exit is completely full. At lower height ratios however, the discreteness of the individual jets from the discharge orifice plates lost their individual identities because of greater length (in terms of the hydraulic diameter or height H). The greater length afforded a more thorough mixing through viscous action to achieve a fuller velocity profile at the exit section.

This phenomenal conjecture was quite well confirmed by the experimental survey of the velocity profiles at the exit section to be discussed next.

c. Exit Velocity Distribution

The measurement of the exit velocity profile was accomplished by a standard total Pitot tube at the mid-section (in Z-direction) of the exit plane. Approximately 15 points were surveyed starting from the ground board upward. This velocity survey, however, was conducted only for some typical runs in order to assess the hypothesis of partial flow at the exit station as was discussed previously.

From these observed velocity-head readings two distribution curves were shown in Figures 26 and 27. For a small height ratio H/L = 0.1 (Figure 26) the velocity profile at the exit was completely full. At low values of $C_d A_r$, i.e. A_r = 0.0599, the velocity distribution resembled most what was predicted in Part I - Theory. For a larger height ratio H/L = 0.6 (Figure 27) the flow was almost confined near the lower half the flow cross section. This essentially confirmed the points discussed in the preceding section.
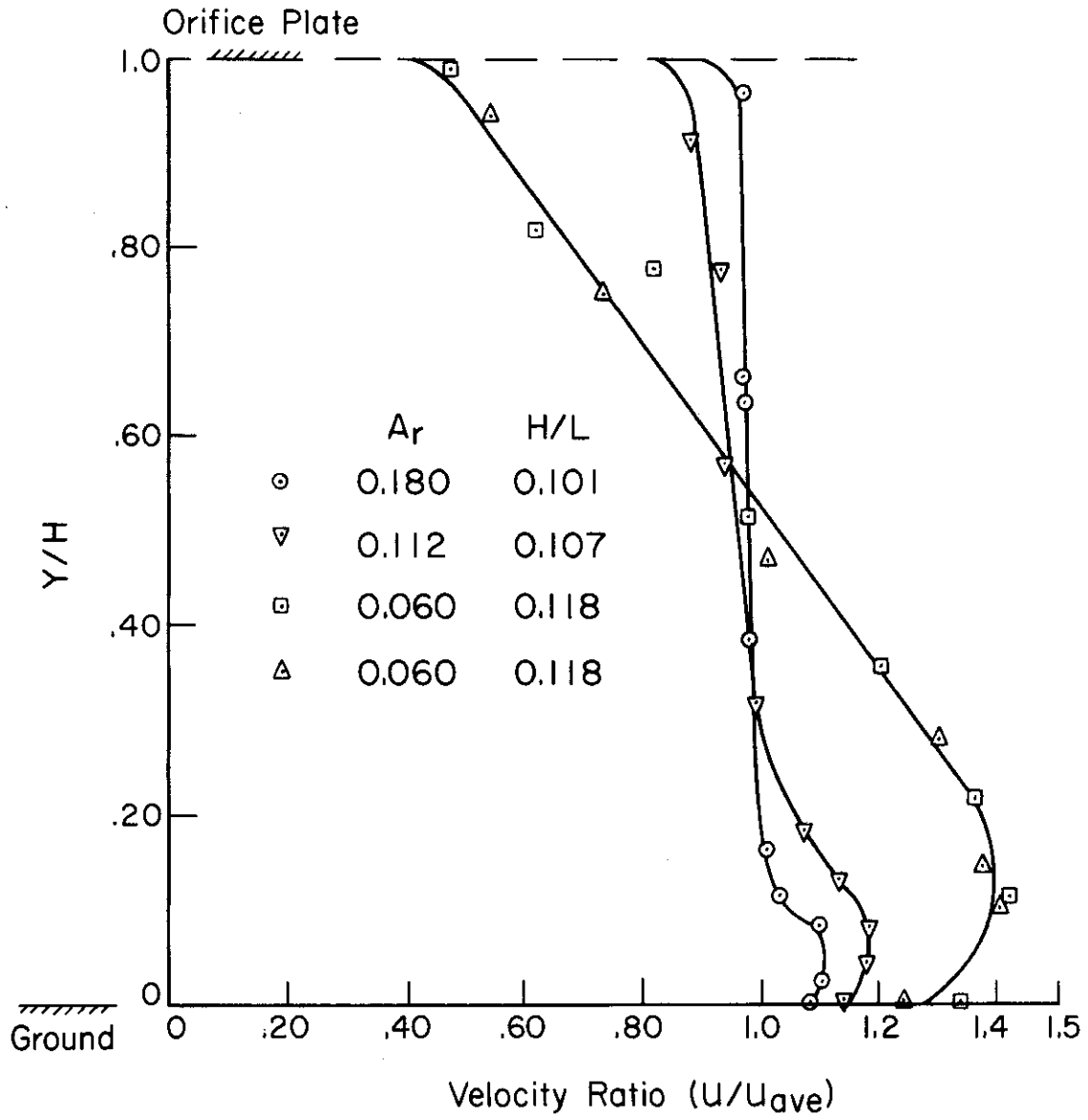
Orifice Plate

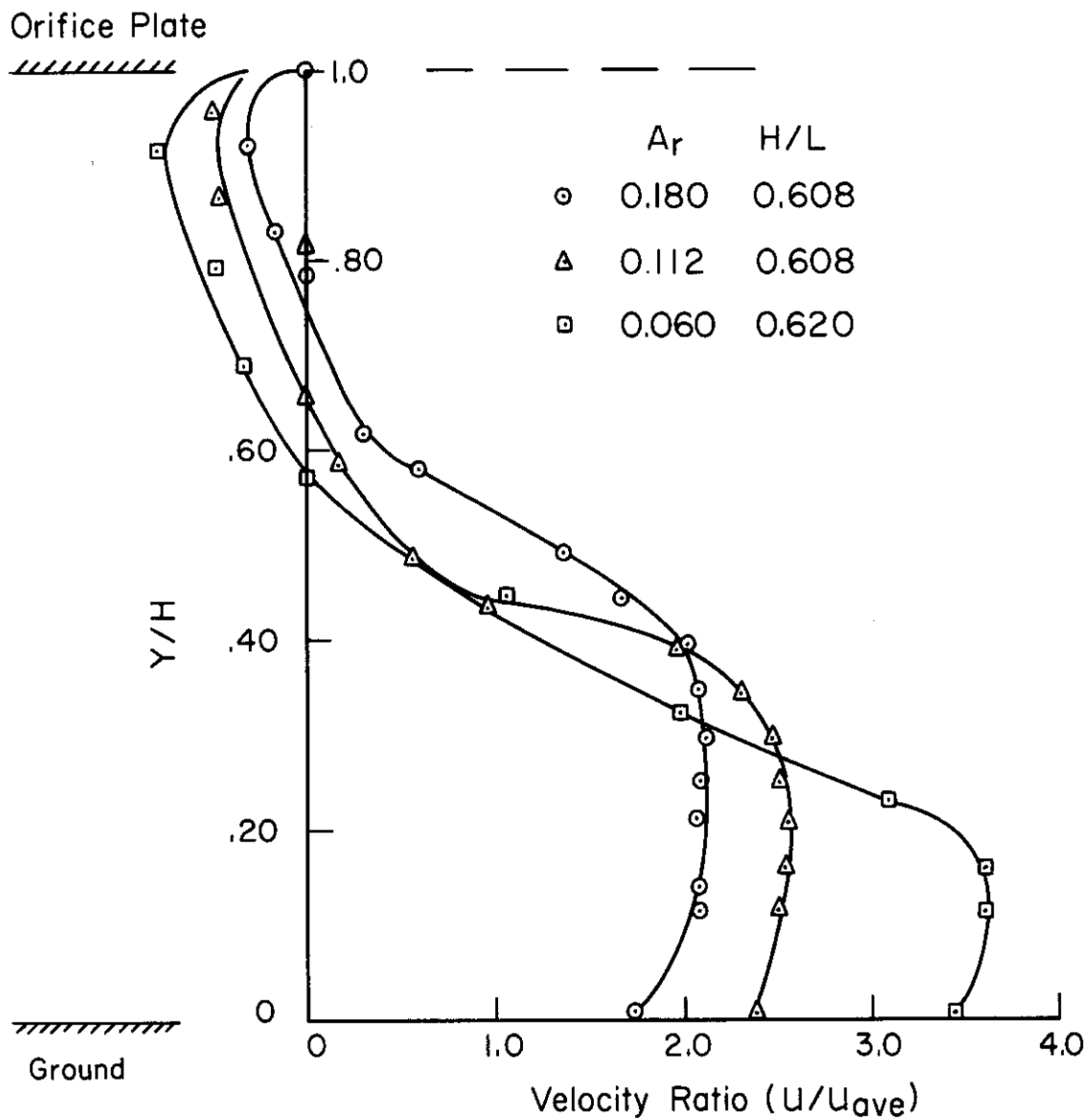FIGURE 26. Velocity Profile At Cushion Chamber Exit.
(H/L = .1)

FIGURE 27. Velocity Profile at
Cushion Chamber Exit
(H/L = 0.6)

V. CONCLUSIONS

The following conclusions can be drawn concerning the results of this experiment:

1. The cushion pressure ratio, and the cushion pressure distribution ratio are all independent of the mass flow rate within the range of the mass flow rates used in this experiment.

2. The theory developed in Part I gave excellent to good results at low height ratio (0.1) but only fair results at (H/L) = 0.3 or greater. At larger height ratios, a multi-peripheral jet theory is expected to apply.

APPENDIX I

CALIBRATION OF MULTI-ORIFICE ASSEMBLY

Orifice Discharge Coefficient

The purpose of this part of experimentation was
to determine the coefficient of discharge of a single
orifice within a matrix of identical orifices as a function
of Reynolds number and geometry. The coefficients obtained
were compared with that for a concentric, single hole
orifice plate having an orifice diameter equal to that of
the matrix orifice.

Specifically, the multi-holed plates considered
in this study were plates prepared with multiple orifices,
all orifices conforming to standard ASME specifications for
edge thickness, etc. The geometric parameters influencing
the value of the discharge coefficient of the orifices in
the matrix, and considered in this investigation were:

(1) Orifice pitch ratio

(2) Orifice pattern

(3) Orifice diameter

The discharge coefficients were correlated with these
parameters and with the Reynolds number based on the
diameter of the orifices in the matrix. The Reynolds
numbers studied ranged from approximately 11,000 to 300,000,
depending on the geometry being tested. In total, sixteen

experimental plates were prepared to examine the effects

produced by the various geometric parameters, and Reynolds

number.

In the following sections, a description of the

test facility, experimental orifice plates, and general

operating procedures are detailed. The calculations

necessary to obtain the discharge coefficients are also

outlined, along with an accuracy analysis of the results.

Test Apparatus

The primary elements comprising the test facility

for this investigation were a laboratory piping circuit, a

standard flow rate measuring test section, the experimental

test section, and the experimental orifice plates to be

studied. Each of these elements will be described below.

a. Laboratory Piping Circuit

Figure 28 is a schematic drawing of the laboratory

piping arrangement showing the flow metering section and

the experimental test section. To insure accurate measure-

ments of the flowing fluid it is necessary that the velocity

profile upstream of the orifice be fully turbulent. To

produce such a condition there are published data on the

recommended minimum lengths of straight pipe that are to

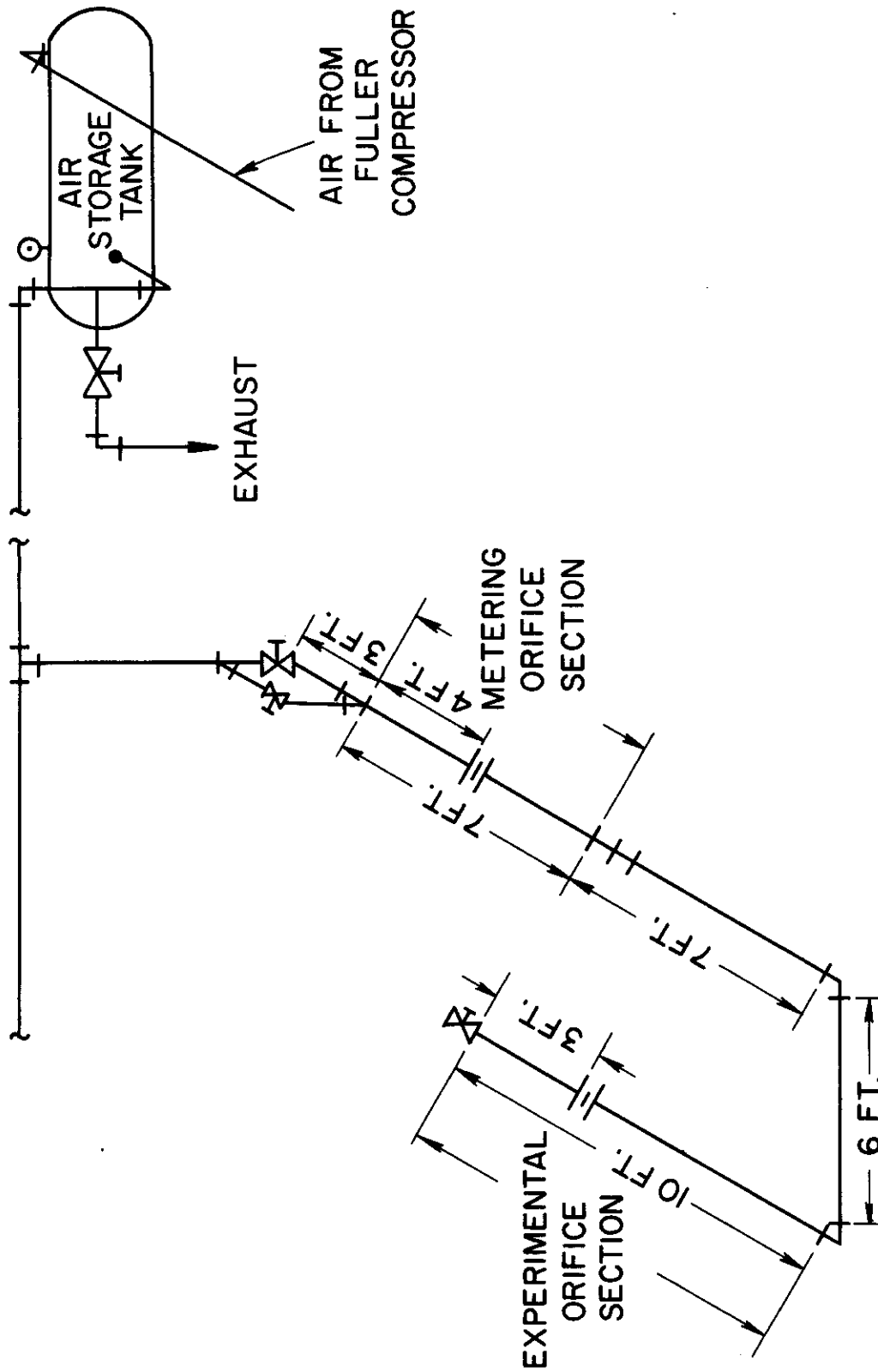precede and follow the orifice plate. In all cases these

FIGURE 28. LABORATORY PIPING CIRCUIT FOR ORIFICE COEFFICIENT TEST

minimum lengths were exceeded. In addition, new pipe was used to minimize any effects that could be produced by pipe roughness. Commercial 4.0-inch steel pipe with threaded ends to accommodate threaded 150 pound cast iron flanges was selected. Standard pipe was chosen so that results obtained in this experiment could be easily reproduced.

Air was delivered to the piping circuit by a 200 horsepower Fuller air compressor. Flow rates ranging from 0.15 to 1.6 pounds per second were used during the investigation, maximum compressor output being 1.9 pounds per second at 40 psig. These flow rates resulted in Reynolds numbers in the range of 35,000 to 580,000 based on the measured internal pipe diameter of 4.026 inches.

b. Flow Metering Test Section

The rate of flow through the piping circuit was measured by a thin-plate standard concentric orifice. This plate was machined from type 304 stainless steel with the orifice diameter measured at 2.124 inches. A sixty-inch single tube water manometer and a twenty-four-inch mercury manometer were used to measure the pressure differentials across the orifice plate. Flange pressure taps were employed in conjunction with the manometers. The static pressure upstream of the orifice plate was measured by a Bourdon type pressure gauge with a pressure range from

0 to 60 psig. Temperature of the air was measured at 3 diameters downstream of the plate with a 0-120 degrees F partial immersion thermometer inserted directly into the middle of the flow stream.

Choice of the diameter ratio for this metering orifice was based on the flow rate range to be covered. Upon examination of the ASME Fluid Meters (Fluid Meters – Their Theory and Application, Am. Soc. of Mech. Engrs., New York, 1959) tables for K (coefficient of discharge divided by the velocity of approach factor) versus Reynolds number it was found that for the diameter ratio in question, flow rates and pipe diameters yielding a Reynolds number of 10,000 or greater could be investigated with the quoted ± 0.555 percent accuracy. Thus the diameter ratio of 0.5125 allowed accurate flow measurements for the Reynolds number range studied in this program.

c. Experimental Orifice Plate Test Section

The experimental test section was essentially constructed like the metering section. Pressure differentials across the experimental plates were measured with sixty inch single tube manometers. Either mercury or water was incorporated as manometer fluid due to the great range of pressure drops found across the test orifice plates.

Flange taps were employed here as well. Temperature
measurement was made by a copper-constantan thermocouple
in this case. The measurement was made five diameters
downstream of the test plates with the thermocouple bead
inserted mid-stream of the air flow. The static pressure
was measured upstream of the test orifice plates by a
Bourdon type pressure gauge, pressure range from 0 to 60
psig. As with the metering section, pressures measured
at the flange taps were transmitted to the manometers by
1/14 inch ID flexible tubing.

d. Experimental Orifice Plates

To thoroughly study the effects of orifice
"crowding", the experimental plates were designed to (1)
show the effect of orifice matrix pattern, and (2) show
the effect of increased density of the orifice holes on
one plate. To these objectives the plates were designed
with orifices arranged in either a square or triangular
pattern, orifice diameters of either 1/2 inch or 5/8 inches,
and center-to-center pitch ratios from 3.0 to 1.25. The
exact tabulation is as follows.

EXPERIMENTAL ORIFICE PITCH TABULATION

Orifice Dia. = 1/2 Inch		Orifice Dia. = 5/8 Inch	
Square Pattern	Triangular Pattern	Square Pattern	Triangular Pattern
3.0	3.0	2.5	2.5
2.0	2.0	2.0	2.0
1.5	1.5	1.5	1.5
1.25	1.25	1.25	1.25

Since the test data were to be compared with those for a standard ASME orifice plate with a single orifice having the same diameter as that of the test orifices it was decided to machine the orifices in accordance with ASME standard practices. Subject to those restrictions the plates were manufactured from 3/32 inch thick aluminum plate with the orifice edge beveled to 1/32 of an inch. Figure 29 shows the dimensions specified for a typical plate. The upstream edges were de-burred so as not to destroy the sharp edge. Photographs of the plates are listed in Figure 30. Note that the plates were manufactured from aluminum plate and not one of the orifice materials as suggested by the ASME. It was felt that since these plates would probably be used only once, the cost and machining problems associated with the standard
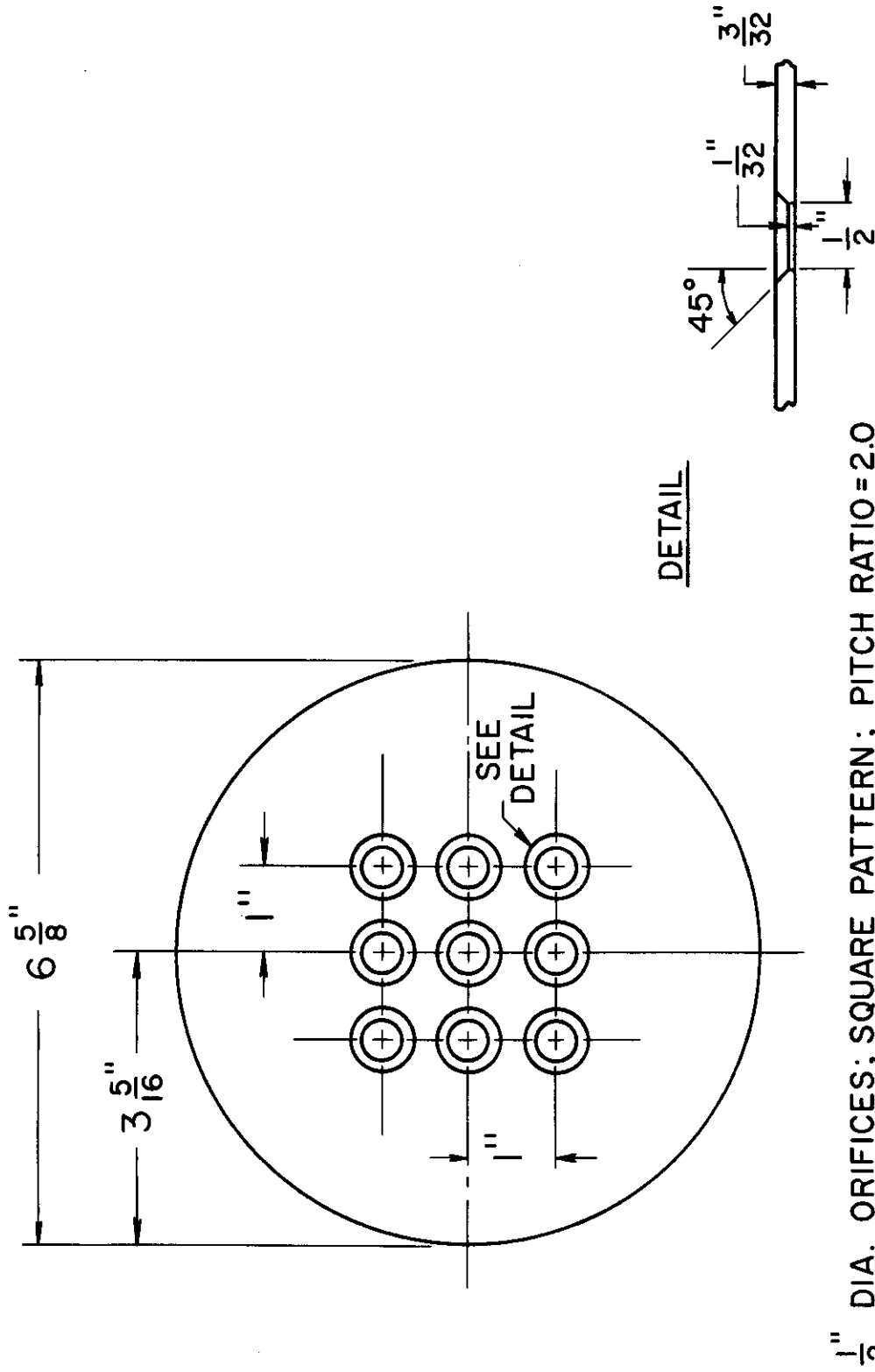
$\frac{1}{2}''$ DIA. ORIFICES; SQUARE PATTERN; PITCH RATIO = 2.0

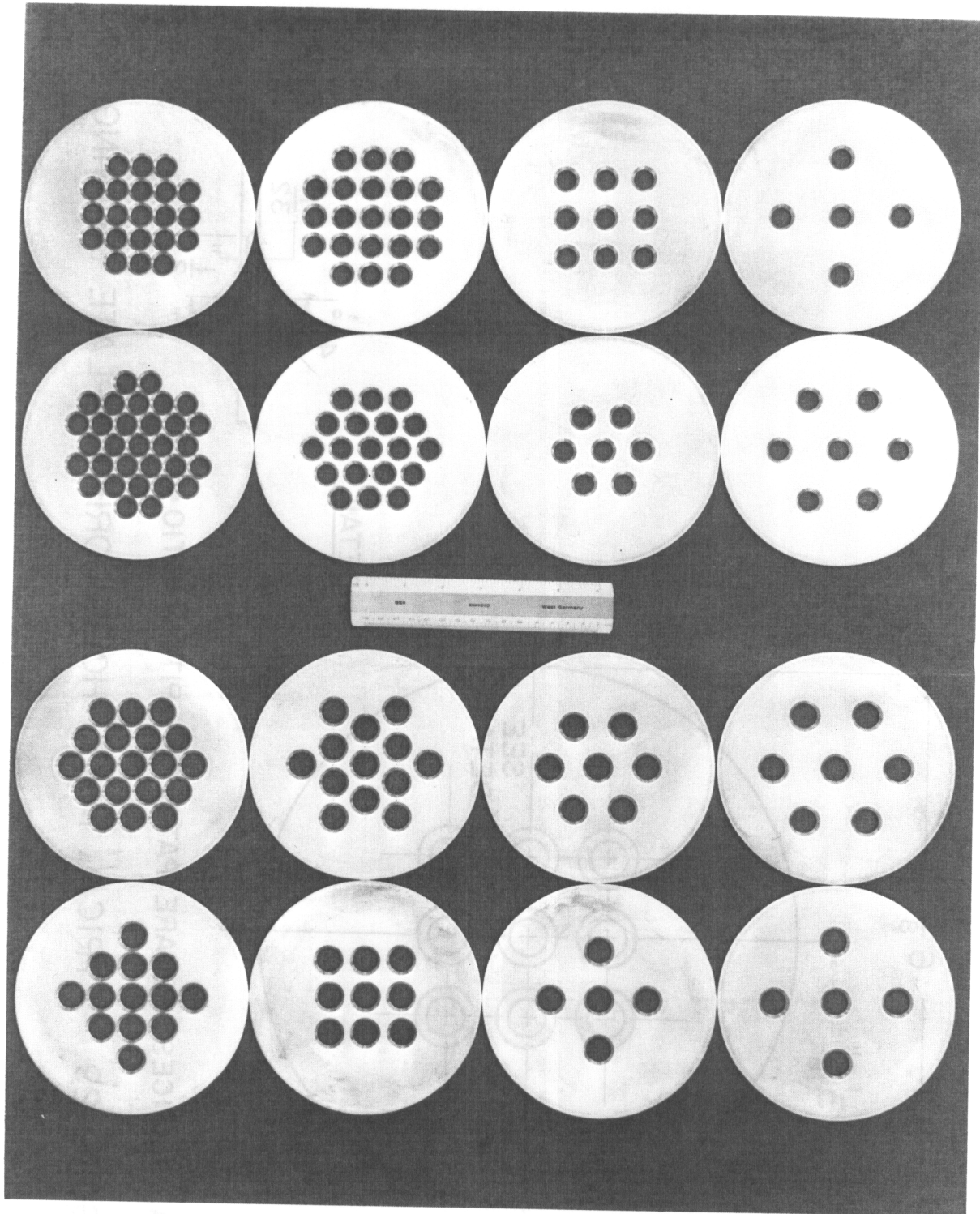FIGURE 29. TYPICAL MULTI-HOLED ORIFICE PLATE DRAWING

DETAIL

$\frac{3}{32}''$

$\frac{1''}{32}$

$\frac{1''}{2}$

45°

$6\frac{5}{8}''$

$3\frac{5}{16}''$

$1''$

$1''$

SEE DETAIL

Figure 30   Upstream View of Test Orifice Plates

orifice plate materials were unjustified. Therefore,
aluminum appeared to make the best compromise.

Data Reduction

The purpose of this section is to discuss the
manner in which the data obtained in this study was con-
verted to provide some meaningful results. The inaccuracies
that were present in the calculations will also be reviewed.
The primary result of this investigation was the calculation
of the coefficient of discharge for a single orifice in a
matrix of orifices. The theory behind the calculations,
and the manner in which the computations were carried out
are the topics of discussion in this section.

By definition, the coefficient of discharge of an
orifice is the ratio of the actual rate of flow to the
theoretical rate of flow passing through that orifice. It
is essentially a measure of the efficiency of the orifice.
In order to calculate its value, both the actual and
theoretical rates of flow must be known. Thus, the objective
of the data acquisition program for this investigation was
to provide the proper information for a precise determination
of both rates of flow. The theoretical weight rate of flow
through a thin plate concentric orifice can be calculated
by the following equation:

$$W_H = \frac{359.0 \, d^2}{\sqrt{1-\beta^4}} \sqrt{h_w \gamma} \qquad (1)$$

To obtain the actual flow rate through the orifice, this equation is multiplied by the discharge coefficient, C_d. That is

$$W_H = \frac{359.0\ C_d d^2}{\sqrt{1-\beta^4}}\ \sqrt{h_w \gamma} \qquad (2)$$

Where:

h_w = pressure drop across the orifice plate, inches of water

γ = specific weight of flowing fluid lb/cu ft

d = orifice diameter

β = orifice-to-pipe diameter ratio.

Equation 1 is derived from Bernoulli's equation. Equation 2 can be altered in the following way: multiplying the right hand side of the equation by D^2/D^2, and noting that $\beta^2 = d^2/D^2$, equation 2 becomes

$$W_H = \frac{359.0\ C_d \beta^2 D^2}{\sqrt{1-\beta^4}}\ \sqrt{h_w \gamma}$$

where D = pipe diameter.

Now by letting $K = C_d / \sqrt{1-\beta^4}$ and $I = 359.0\ K\beta^2$, the expression can be written as

$$W_H = D^2\ I\ \sqrt{h_w \gamma} \qquad (3)$$

Since the ASME (Computation Handbook, New York, Am. Soc. of Mech. Engr., 1959) tabulates the parameter I for various diameter ratios β, it was this equation that was used to

calculate the actual weight rate of flow through the system.
Certain limitations are placed on the use of this equation,
however. First, the flow is assumed to be incompressible.
Second, the area of the orifice is assumed to be independent
of the stream temperature. And third, the discharge
coefficient (buried in the Constant I) is assumed not to
vary with the Reynolds number. Since the second and third
conditions described above were known not to exist, correction
factors that compensated for those effects were applied to
equation 3 . In addition, since air was used as the
operating fluid, the first limitation was also seen not to
hold. A correction factor here also was used to compensate
for the compressibility of air. These correction factors
are Y (expansion factor), F_A (area factor), and F_R
(Reynolds number factor). Incorporating these factors,
equation 3 becomes

$$W_H = F_A \ F_R \ Y \ D^2 \ I \ \sqrt{h_w \gamma} \tag{4}$$

This then, was the form of the equation used in the computer
program to determine the actual flow rate passing through
the system.

With the determination of the actual flow rate
in the system, the matter of calculating the coefficient of
discharge became straightforward. Since the coefficient for
one orifice in a matrix of orifices was to be computed, all

69

that need be known about that orifice was the actual and theoretical flow rates through it. The theoretical flow was found by using the data recorded for the experimental plate and equation 1 . The actual rate of flow, assumed to be equal for all matrix orifices, was calculated as the total actual flow rate (equation 4) divided by the number of orifices in the matrix. Thus, the equation used to determine the coefficient of discharge for one orifice in the matrix was

$$C_d = \frac{\left[F_A \ F_R \ Y \ D^2 \ I \ \sqrt{h_w \gamma} \right]_{meter}}{n \left[\dfrac{359.0 \ F_A \ Y \ d^2}{\sqrt{1-\beta^4}} \right] \sqrt{h_w \gamma}_{\ test}} \qquad (5)$$

Since this coefficient was to be determined as a function of the Reynolds number of the orifice, a great number of trials needed to be made on each of the sixteen experimental plates. Subject to this it was felt that the only efficient method of handling the data was via computer.

Test Results

It was convenient to express the variation in the coefficient of discharge for one orifice within a matrix of similar orifices for various (1) orifice pitch ratios, (2) geometric spacing, and (3) orifice diameters, as a function of the Reynolds number based on the orifice diameter.

As noted under <u>Test Apparatus</u>, sixteen multi-holed orifice plates were made in order to study the effects of decreased orifice pitch, spacing, and diameter, on the discharge coefficient. In this section the effect of each parameter on the experimentally determined discharge coefficient will be examined. In addition, the total effect of all the parameters acting together will be discussed.

a. Effect of Increasing Pitch Ratio

The experimentally determined coefficients of discharge as a function of the Reynolds number based on the orifice diameter are given in Figures 31 through 38. The reference value shown on these figures was the discharge coefficient for a single orifice and was included therein for comparison. These results show that, for plates with the same orifice diameter, the coefficient of discharge increases for a decreasing pitch ratio. The individual cases are examined below.

In reference to the plates having 1/2 inch diameter orifices, for the pitch ratios of 3.0 and 2.0 the discharge coefficient did not appreciably vary with the Reynolds number based on the orifice diameter (here-after called the orifice Reynolds number). For these ratios the discharge coefficient remained at a value of

approximately 0.62 for orifice Reynolds numbers in the range
of fifty to three hundred thousand. There was little
scatter about this value for either geometric spacing of
orifices. For this same range of orifice Reynolds numbers
the coefficient of discharge for a single, thin plate, 1/2
inch diameter concentric orifice was calculated to be
0.5953. This value served as a reference value to which
the coefficient for the test plates could be compared. This
reference discharge coefficient was computed from equations
given in the ASME Fluid Meters Report. When the pitch was
decreased to 1.5 the value of discharge coefficient increased
to an average of 0.66 for both spacings. In the equilateral
arrangement, the coefficient once again did not vary with
the orifice Reynolds number over the range studied. The
result for the square spacing was quite similar except for
an abrupt "hump" in the curve in the orifice Reynolds number
range one hundred to one hundred and eighty thousand. This
peculiarity will be discussed in the next section. As was
the case when the pitch ratio was reduced from 2.0 to 1.5,
a reduction in the ratio from 1.5 to 1.25 further increased
the coefficient for both patterns. For the square spacing,
the coefficient increased from approximately 0.675 to about
0.680. Once again this value remained independent of the
Reynolds number over the entire range. In the equilateral
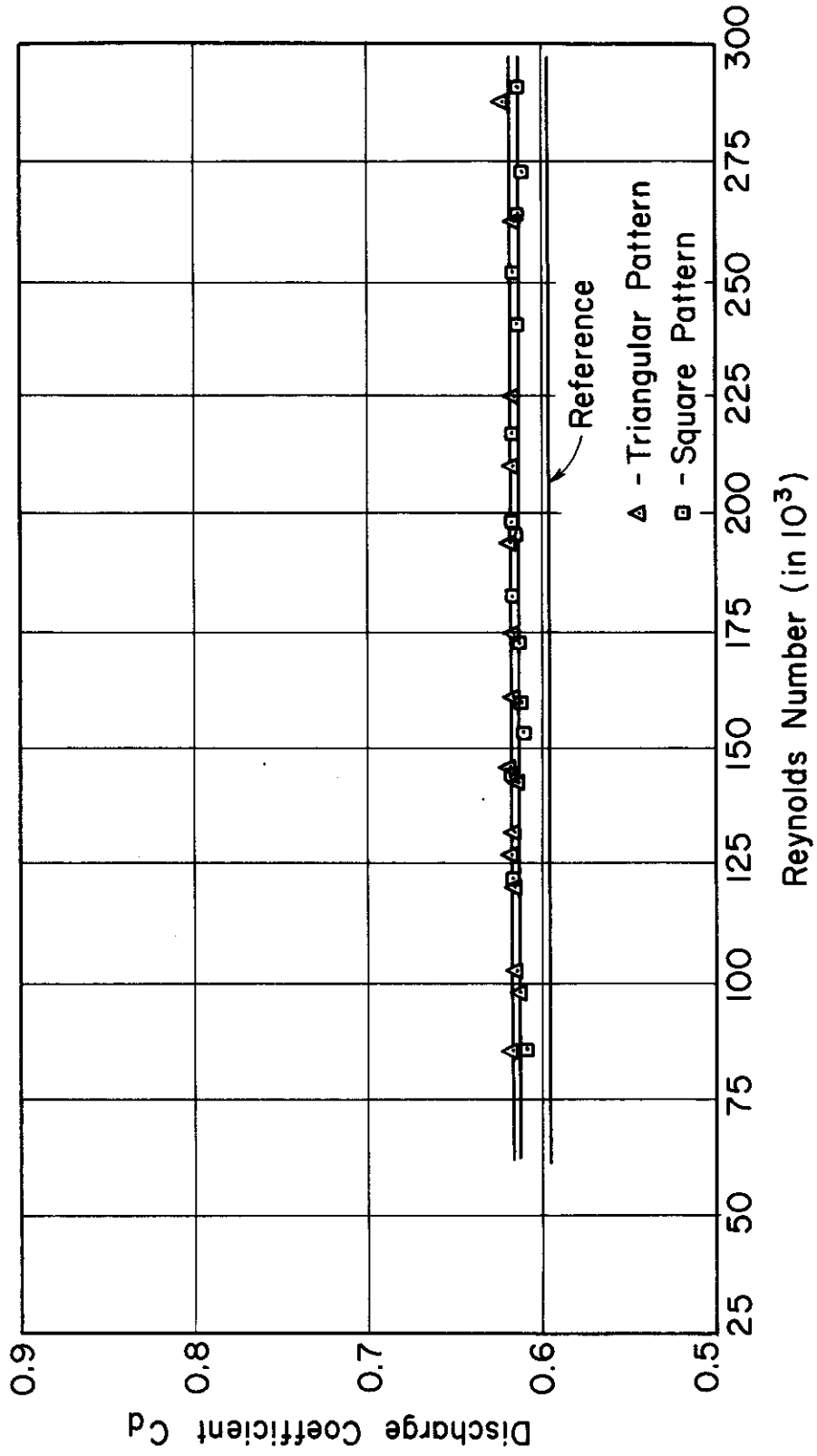spacing, however, a very extraordinary result appeared.

FIGURE 31. Discharge Coefficient for Orifice Diameter $\frac{1}{2}$ inch. (Pitch = 3.0)
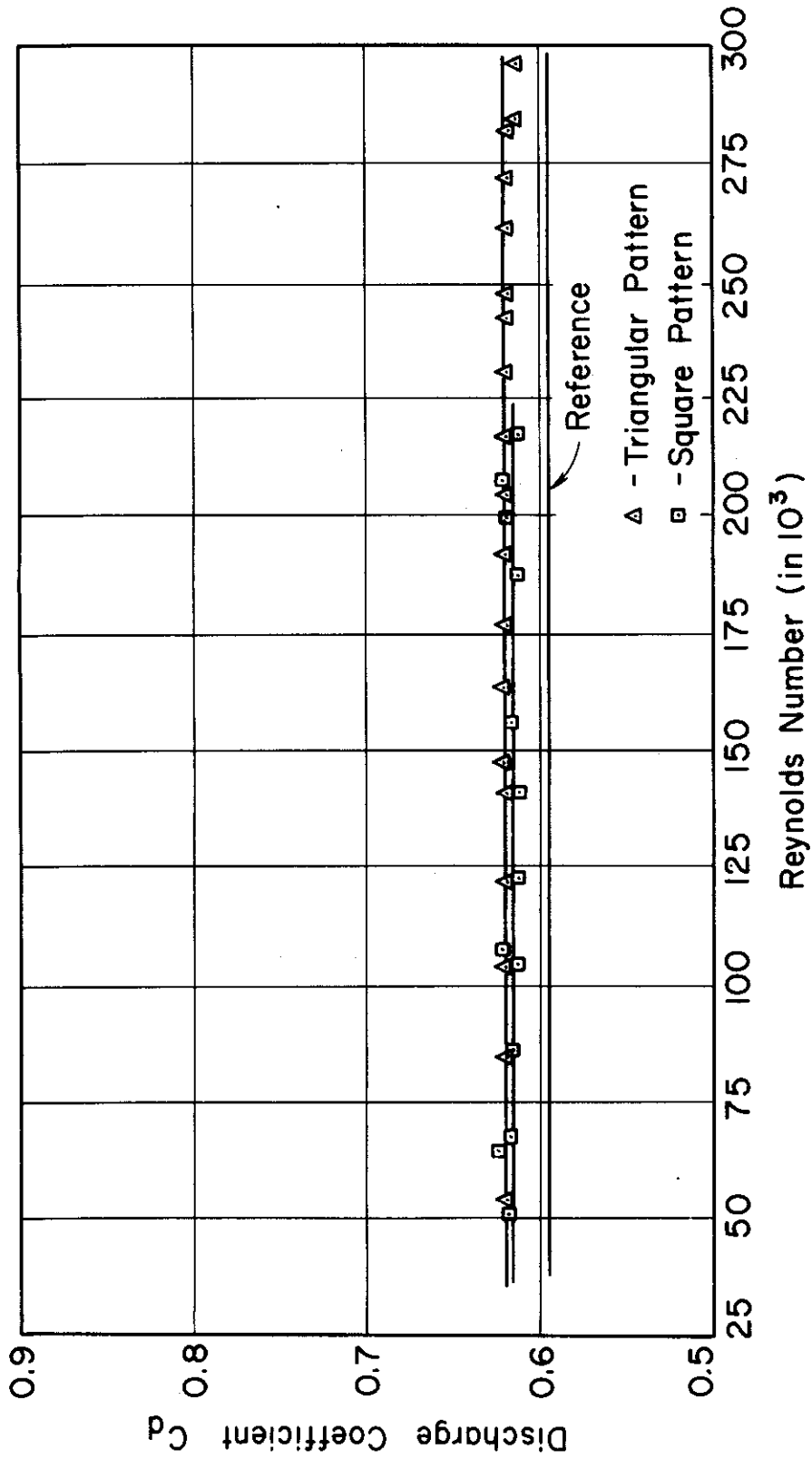
FIGURE 32. Discharge Coefficient for Orifice Diameter $\frac{1}{2}$ inch. (Pitch = 2.0)
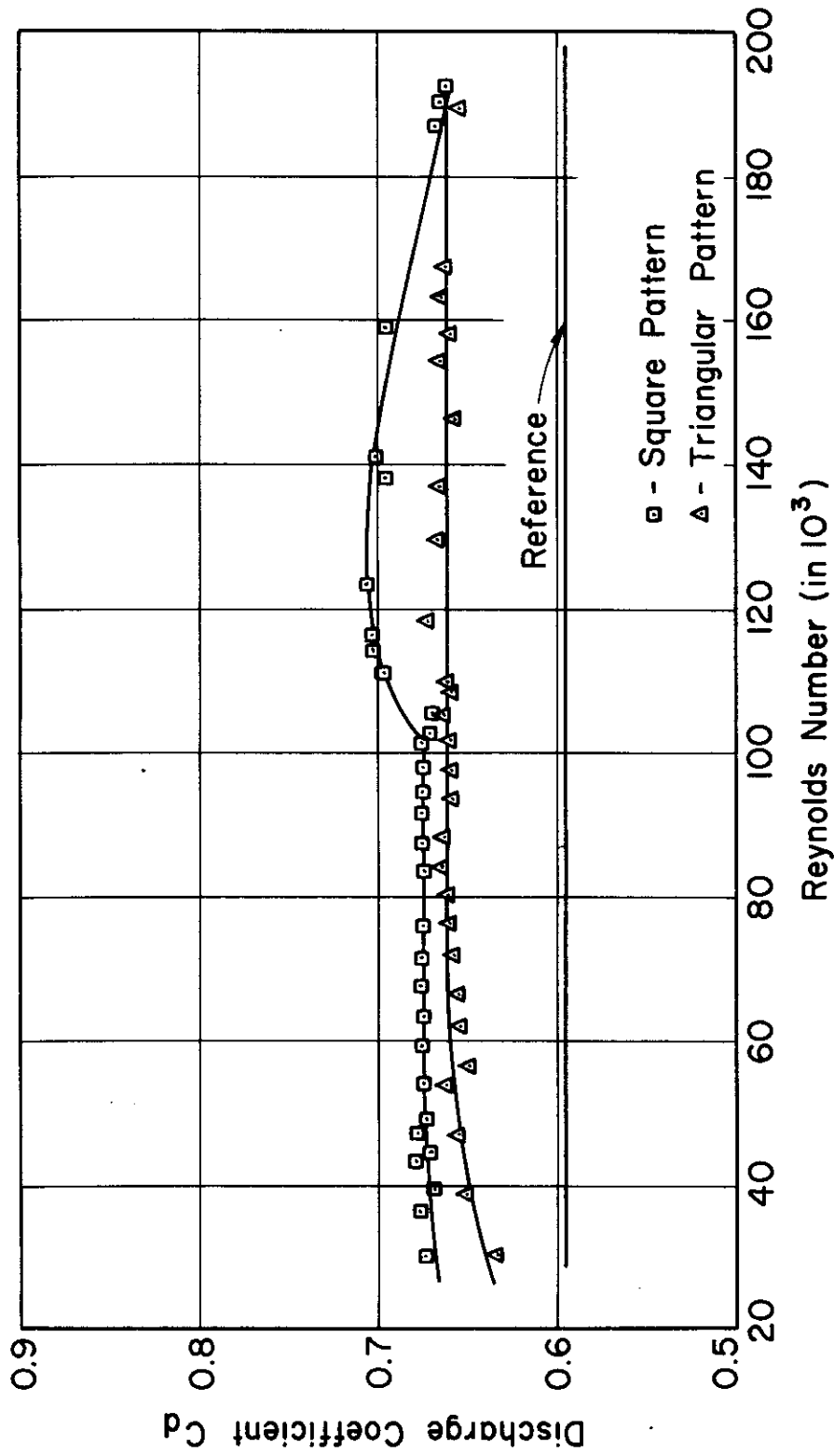
FIGURE 33. Discharge Coefficient for Orifice Diameter $\frac{1}{2}$ inch. (Pitch = 1.5)
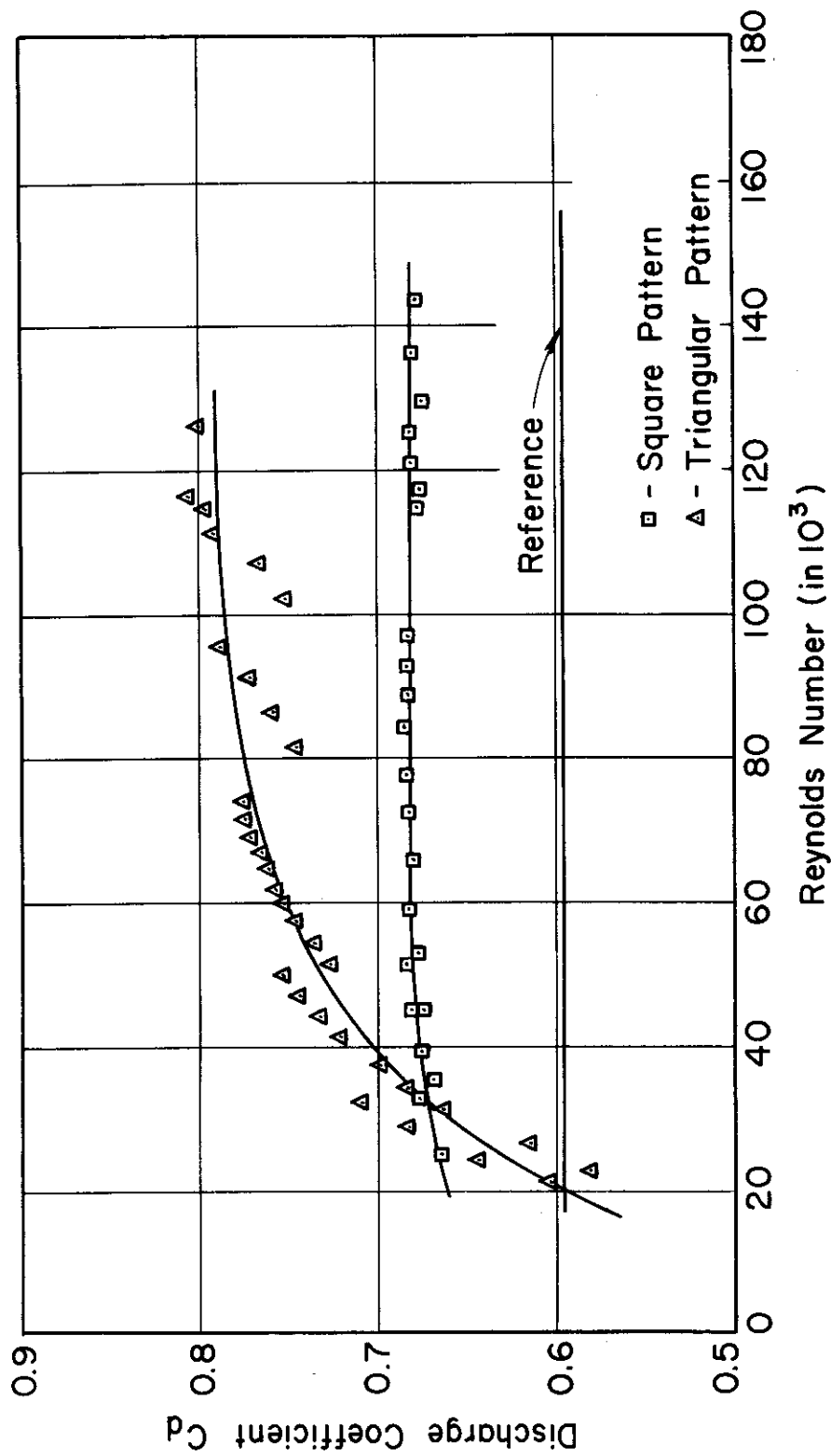
FIGURE 34. Discharge Coefficient for Orifice Diameter $\frac{1}{2}$ inch. (Pitch = 1.25)
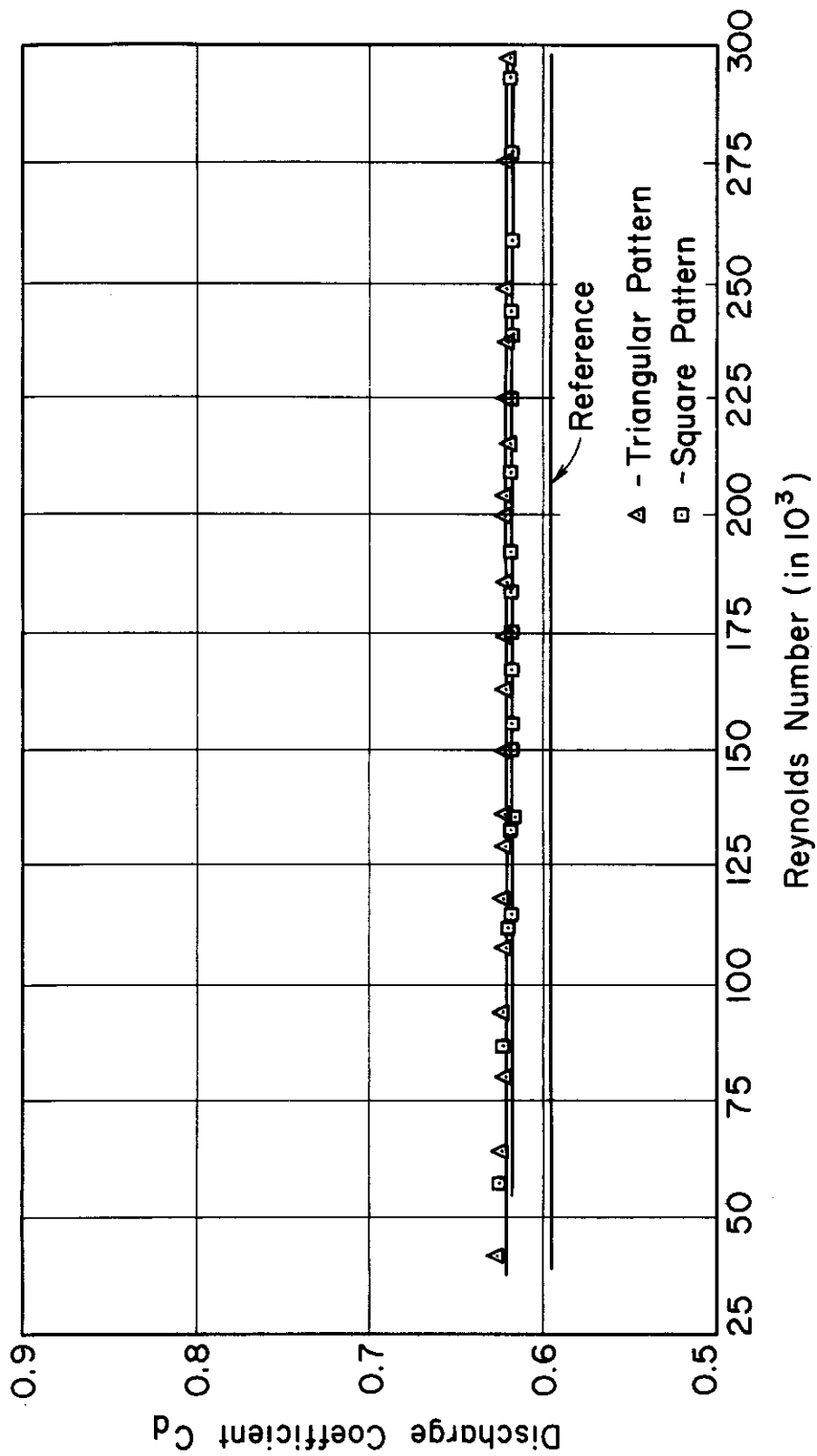
FIGURE 35. Discharge Coefficient for Orifice Diameter $\frac{5}{8}$ inch. (Pitch = 2.5)
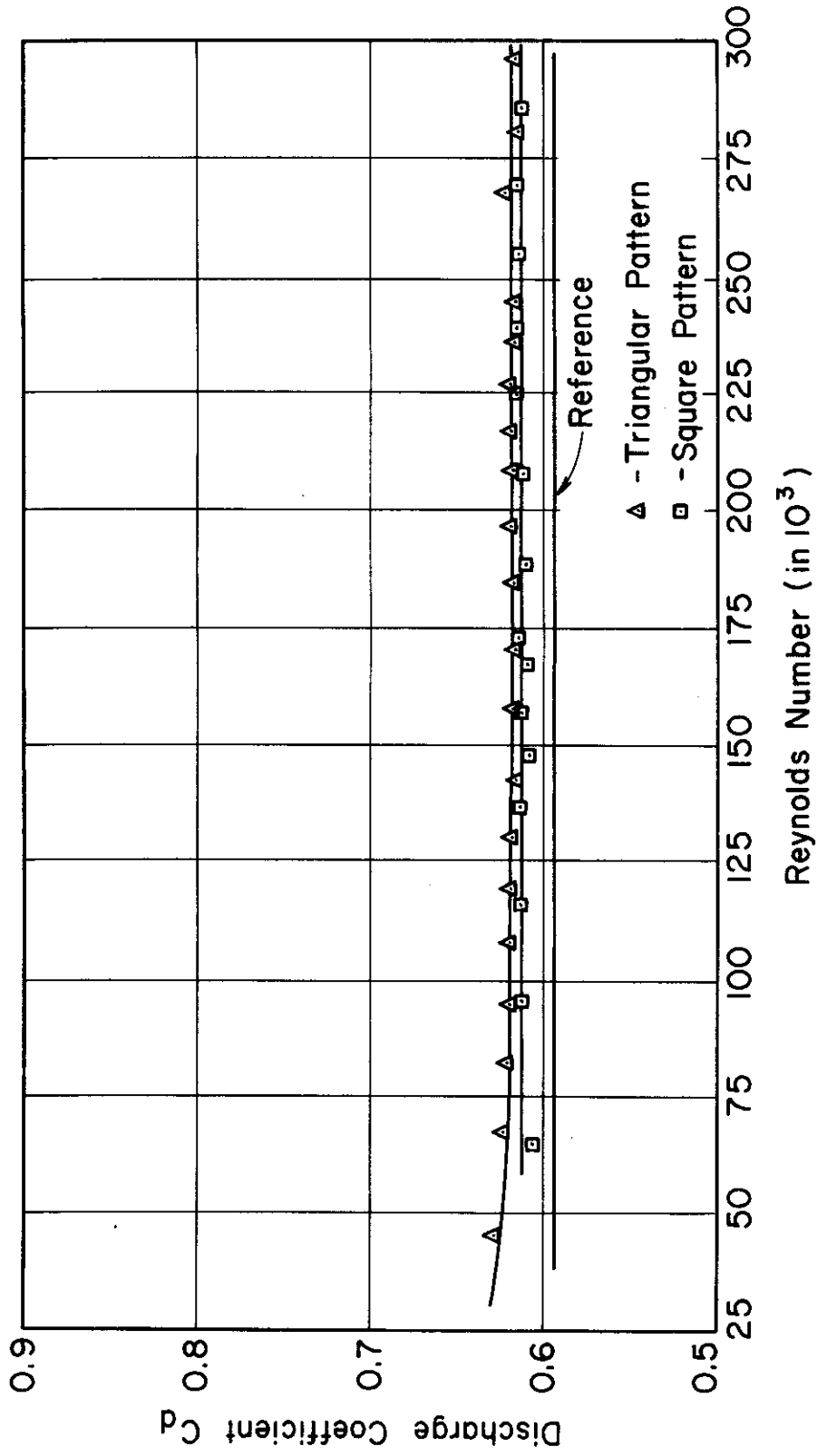
FIGURE 36. Discharge Coefficient for Orifice Diameter $\frac{5}{8}$ inch. (Pitch = 2.0)
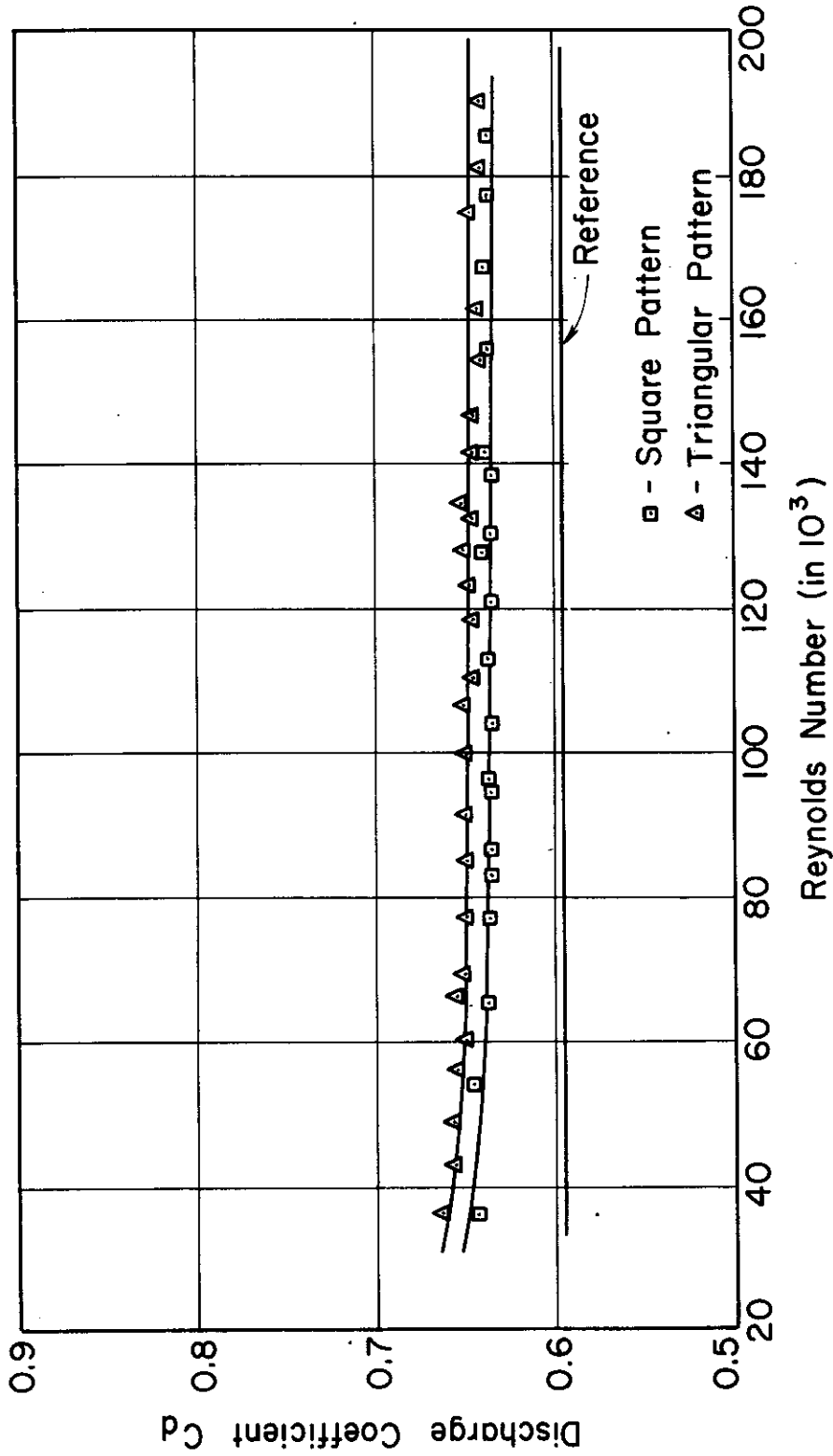
FIGURE 37. Discharge Coefficient for Orifice Diameter $\frac{5}{8}$ inch. (Pitch = 1.5)
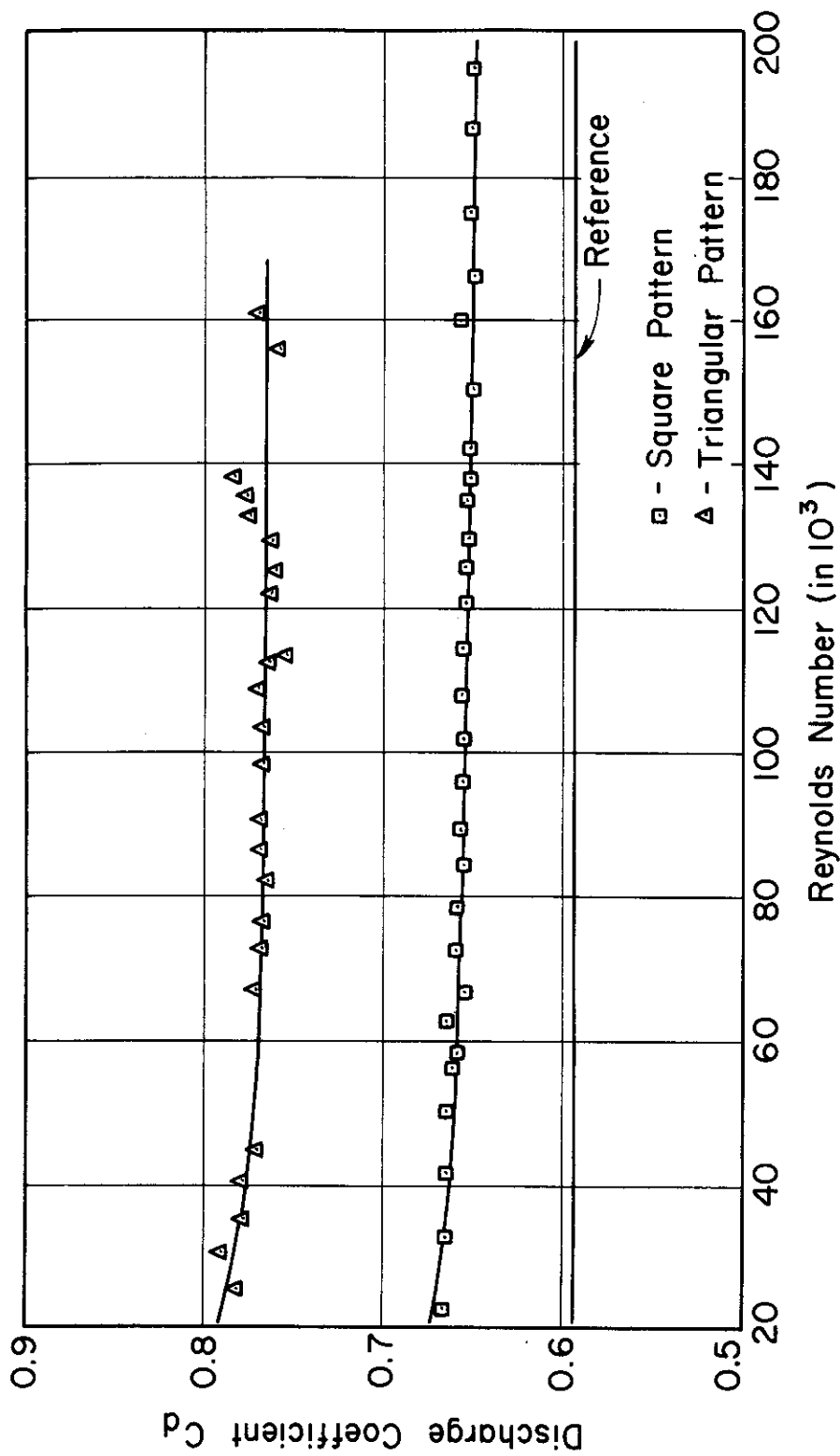
FIGURE 38. Discharge Coefficient for Orifice Diameter $\frac{5}{8}$ inch. (Pitch = 1.25)

Not only did the discharge coefficient increase, but it increased in a very dramatic fashion. Starting at a value of approximately 0.6 at an orifice Reynolds number of twenty thousand, the coefficient climbed to a value of about 0.76 for a Reynolds number of sixty-five thousand. This plate, orifice diameter of 1/2 inch, triangular spacing, and a pitch ratio of 1.25, was the only experimental plate to record such a result. Its curious behavior will also be discussed next.

The trend of increasing coefficients of discharge for decreased pitch ratios continued in the plates having orifice diameters of 5/8 inches. For pitch ratios of 2.5 and 2.0 the coefficient did not vary with the Reynolds number in the range studied. Similar to the 1/2 inch diameter orifices there was little scatter in the calculated result with the average value of the two patterns being about 0.62. The plates having a pitch ratio of 2.0 did show a slight increase in the coefficient compared to those having a 2.5 pitch ratio. The reference coefficient was determined to be 0.5943 for the same Reynolds number range. Identical to the plates having the smaller orifices, when the pitch was decreased to 1.5, a significant increase in the coefficient resulted. The average value was increased from 0.62 to roughly 0.642. The curve was, for the most part, "flat" with a slight upward curvature noted at the

low Reynolds numbers (40,000 - 60,000). At a pitch ratio

of 1.25 the coefficient was still higher. In the square

spacing, the coefficient increased from 0.636 to about 0.655.

The increase for the equilateral spacing was even more

pronounced, the coefficient increasing from about 0.648 to

0.768. In this case, however, the coefficient did not

increase with Reynolds number as was described for the 1/2

inch diameter orifices in the same pattern and ratio.

Here again it was observed that the coefficient was not

influenced by orifice Reynolds number.

b. Effect of Geometric Spacing

The effect of geometric spacing of the orifices

on the plate can also be examined by reviewing Figures 31

through 38. The trend for both sizes of orifices was for

the equilateral spacing to promote higher discharge coeffi-

cient. This effect was amplified at the lower pitch ratios,

or equivalently, for a greater density of orifices in the

plate area. The result obtained for each of the orifice

sizes and pitch ratios will be reviewed below.

The experimental orifice plates with 1/2 inch

diameter orifices did not clearly show increased coefficients

for the triangular spacing arrangement. At the least

crowded conditions, i.e. the pitch ratios of 3.0 and 2.0,

many of the points for one pattern overlapped the curve for

the second pattern. In general however it can be discerned
that in each case the triangular spacing lends itself to a
slightly higher discharge coefficient. The only exception
to this trend, and the one that confuses this issue for the
1/2-inch diameter orifices, occurs at a pitch ratio of 1.5.
In this instance the coefficient was found to be higher for
the square spacing. When the pitch ratio was dropped to
1.25 however, the result observed for pitch ratios of 3.0
and 2.0 was evidenced. Thus for the 1/2-inch diameter
orifices, three plates showed higher coefficients for
triangular spacing, but one plate gave greater coefficients
for the square spacing.

The premise that the equilateral spacing tends to
increase the discharge coefficient was confirmed by the
results obtained on the 5/8-inch orifices. Very similar to
what occurred for the smaller orifices at the higher pitch
ratios a great deal of overlapping of points was found.
But examination of the computer output verified that the
triangular spacing did indeed give higher coefficients
over the range of orifice Reynolds numbers plotted. At a
pitch ratio of 1.5 there was a clear separation of the
curves, the triangular spacing yielding discharge coefficients
2 percent higher than those calculated for the square spacing.
Finally, for the lowest pitch ratio tested, namely 1.25,
the increase jumped to 18.5 percent of the value for the

coefficient at a pitch of 1.5. On the basis of these
results, and those found at the smaller orifice diameters,
it appears that the increased orifice density afforded by
the equilateral spacing of orifices versus the square
arrangement yields higher discharge coefficient.

c.   Data for ACLS Application

For orifice Reynolds number (Ud/u) greater than
5000, the discharge coefficient C_d tends to reach a constant
value. For ACLS application this asymptotic value is
usually the value encountered as judged by the computational
work done in Part I. Therefore these asymptotic values were
plotted against the area ratio A_r defined as the orifice
area divided by the total area of the plate. The tendency
that the triangular pitch orifice pattern gave a higher
discharge coefficient has not disappeared on this plot as
shown in Figure 39. Instead two groups of data seemed to
congregate themselves; they are the 0.5 inch orifice group
and the 0.625 inch group. The value on the left, i.e. at
$A_r = 0$ is of course the value for a single orifice. It is
not certain whether these two lines drawn thereon represent
a definite trend, or experimental scatter or the pipe effect
(pipe diameter used = 4 inches). For the values of A_r and
the orifice diameters of the plates used in the cushion-
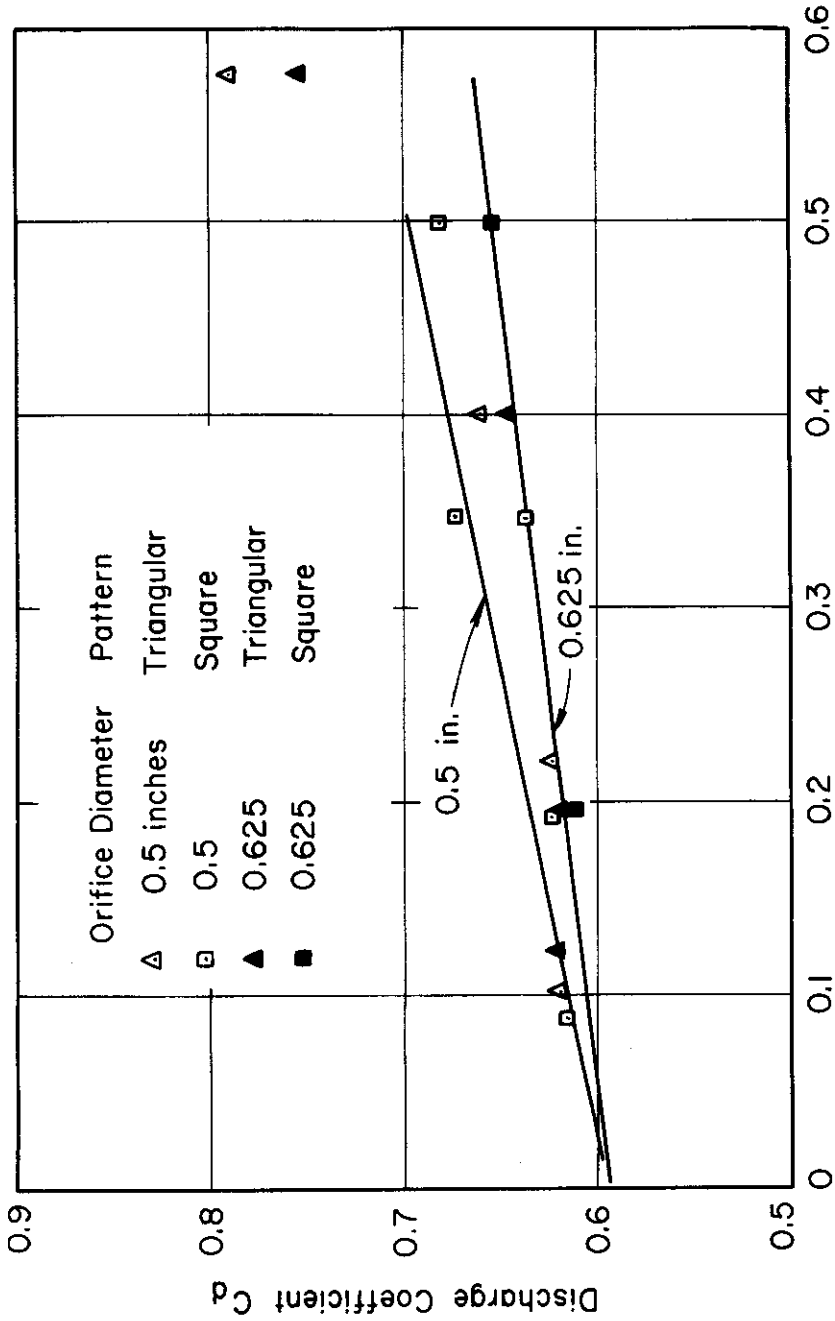pressure experiments the discharge coefficients were

FIGURE 39. Asymptotic Discharge Coefficient vs. Area Ratio

estimated to be 0.620, 0.608, 0.605 respectively for Plate numbers 1, 2, and 3. It was found however a slight variation of C_d of the order 0.010 according to Figure 39 did not change the computed results in the second decimal place.

APPENDIX II

TOTAL PRESSURE VARIATION IN THE SUPPLY CHAMBER

As has been previously mentioned, the total
pressure distribution across the supply chamber in both the
x-direction and the z-direction was not uniform. A survey
was conducted to determine the total variation inside the
supply chamber at various locations along the x-direction
(parallel to the air flow in the channel). The survey was,
however, made at the mid-section of the supply chamber, the
reason being that the variation along the z-direction
(no-flow) was small in view of the data in Figures 10
through 21. The data are plotted in Figures 40, 41, and 42
as the total pressure ratio versus the x-ratio. The total
pressure ratio represents the total pressure measured at a
particular distance (x) from the outside front of the supply
chamber divided by the maximum measured total pressure.
The x-ratio coordinates extended between only 0.15 and 0.85
since between 0 and 0.15 and 0.85 and 1.0 represents the
walls of the supply chamber.

It can be observed from the plot of the data that
the total pressure distribution was dependent upon the
height ratio and upon the area ratio of the orifice plate.
It can also be observed that the larger the area ratio the
greater was the variation of the total pressure ratio.

87

There also seems to be some similarity between the total
pressure distribution and the pressure distribution directly
underneath the multi-orifice plate. This similarity existed
in the form that the total pressure increased from the front
of the supply chamber to a maximum at an x-ratio value of
about 0.60 and then declined to the rear of the chamber
less rapidly than it increased. The pressure distribution
in the clearance space varied likewise.

One of the major reasons for plotting the total
pressure variation data was that a comparison could be
made between the average total pressure and the maximum
total pressure used in the data reduction. In order to do
this, however, it is necessary to know how the total pressure
varied in the z-direction in the supply chamber. No data
were taken concerning the total pressure variation in this
direction but a few observations can be made.

By observing the cushion pressure distribution data
plotted in Figures 10 through 21, it can be seen that the
cushion pressure varied between the average of five to ten
percent in the z-direction at the higher height ratios and
varied under five percent at the low height ratios. Likewise,
the cushion pressure can be observed to vary between fifty
and one-hundred percent in the x-direction depending on
the height ratio while the corresponding total pressure
varied by a maximum of only twenty-five percent. Thus,
based on these observations, it can be concluded that the

total pressure in the supply chamber probably varied slightly in the z-direction and that this variation between the maximum total pressure measured and the average total pressure in the z-direction was probably less than five percent.
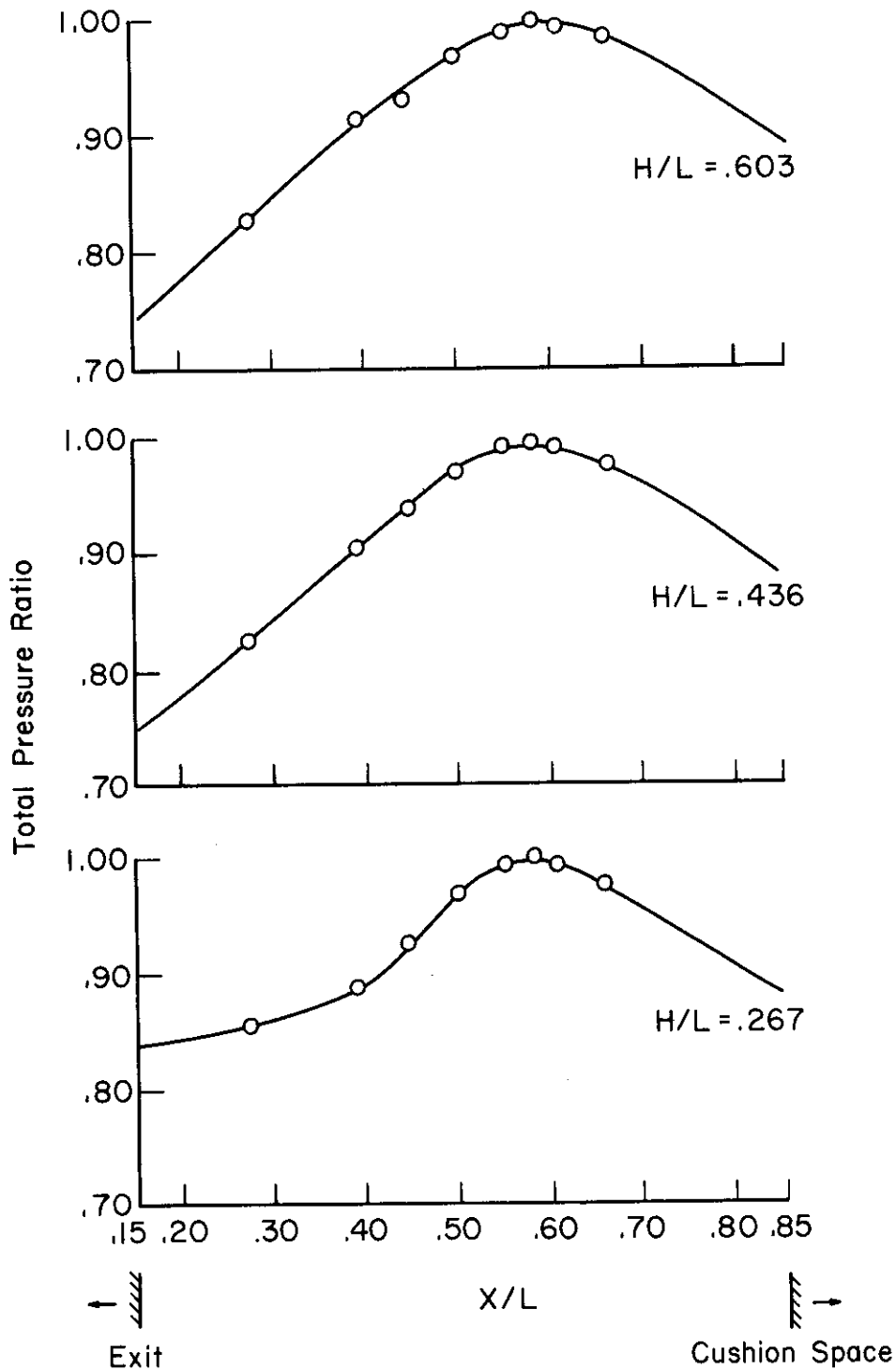
FIGURE 40. Total Pressure Distribution Across
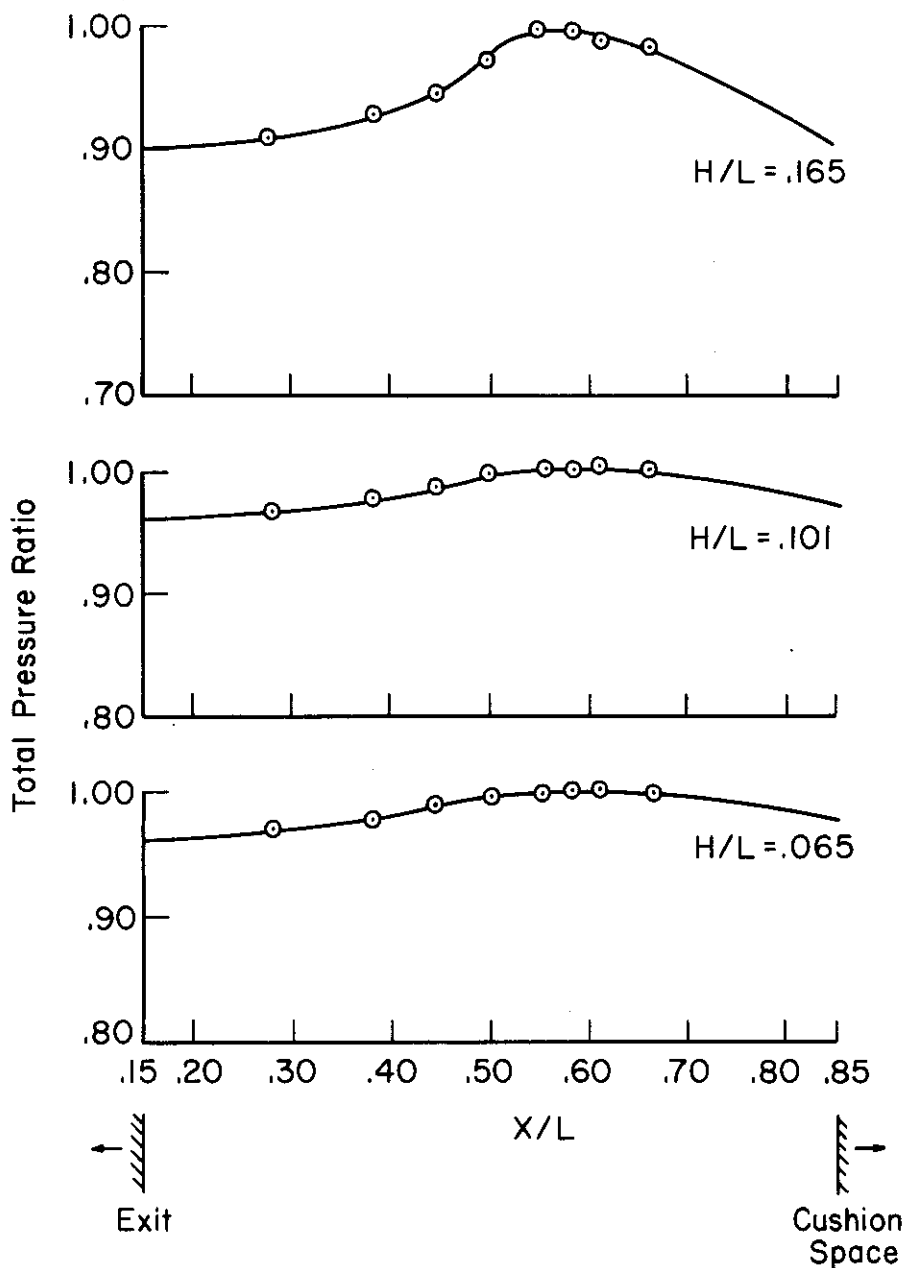Plenum Chamber in x-direction. (A_r = 0.180)

FIGURE 40 Continued.

Total Pressure Distribution Across
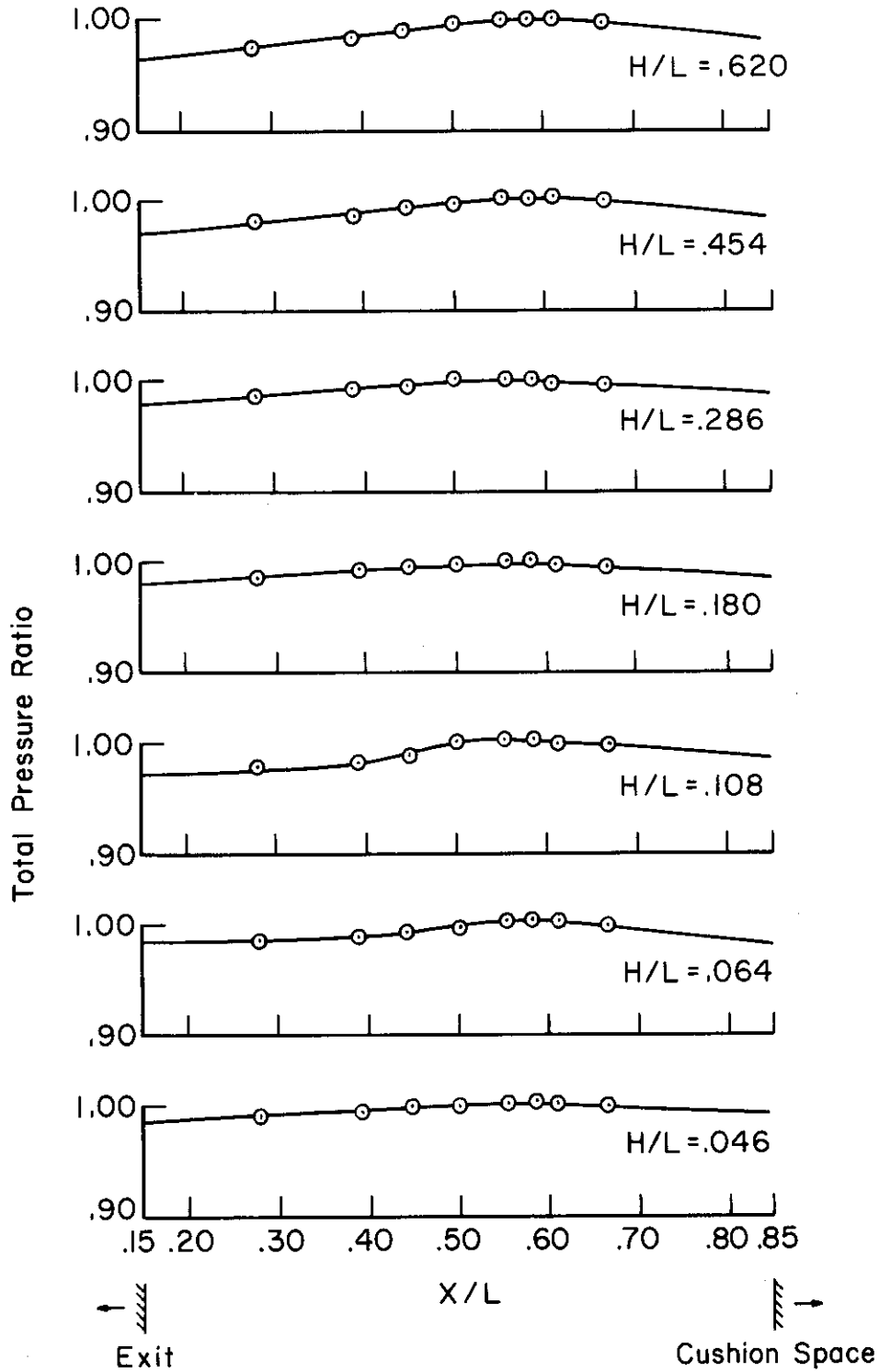Plenum Chamber in x-direction ($A_r = 0.180$)

FIGURE 41. Total Pressure Distribution Across
Plenum Chamber in x-direction ($A_r = 0.120$)

FIGURE 42. Total Pressure Distribution Across Plenum Chamber in-direction. ($A_r = 0.060$)

DOCUMENT CONTROL DATA - R & D

(Security classification of title, body of abstract and indexing annotation must be entered when the overall report is classified)

1. ORIGINATING ACTIVITY *(Corporate author)*	2a. REPORT SECURITY CLASSIFICATION
The Ohio State University Research Foundation Columbus, Ohio	Unclassified
	2b. GROUP

3. REPORT TITLE

Air Cushion Pressure During Stiff-Operation for Air Cushion Landing Systems

4. DESCRIPTIVE NOTES *(Type of report and inclusive dates)*

July 1971 - January 1972 - completion of experimental work, analysis & compilation

5. AUTHOR(S) *(First name, middle initial, last name)*

Professor Lit S. Han

6. REPORT DATE	7a. TOTAL NO. OF PAGES	7b. NO. OF REFS
March 1972	102	2

8a. CONTRACT OR GRANT NO.	9a. ORIGINATOR'S REPORT NUMBER(S)
F33 (615)-70-C-1019	
b. PROJECT NO. 1369	
c.	9b. OTHER REPORT NO(S) *(Any other numbers that may be assigned this report)* AFFDL-TR-71-4, Part II
d.	

10. DISTRIBUTION STATEMENT

Approved for public release; distribution unlimited

11. SUPPLEMENTARY NOTES	12. SPONSORING MILITARY ACTIVITY
	Air Force Flight Dynamics Laboratory Wright-Patterson Air Force Base, Ohio

13. ABSTRACT

This Part II of the report describes the experimental verification of the theory developed in Part I for ACLS in its stiff-mode operation. It also reports the discharge coefficient data required for computing air flow requirements.

At low ground clearances, the theory was verified to be in excellent agreement with the experimental data obtained. At higher values of the ground clearance where the difference between the experimental data and theoretical computation was observed. A multi-jet theory yet to be developed is expected to bridge the gap.

DD FORM 1473
1 NOV 65

14. KEY WORDS	LINK A		LINK B		LINK C	
	ROLE	WT	ROLE	WT	ROLE	WT
Landing gear; ACLS; Launching and alighting Systems; air bearings						